Contrib Mineral Petrol (2013) 166:587–613
DOI 10.1007/s00410-013-0893-2

ORIGINAL PAPER

Magma mixing and the generation of isotopically juvenile silicic magma at Yellowstone caldera inferred from coupling ^{238}U–^{230}Th ages with trace elements and Hf and O isotopes in zircon and Pb isotopes in sanidine

Mark E. Stelten · Kari M. Cooper · Jorge A. Vazquez · Mary R. Reid · Gry H. Barfod · Josh Wimpenny · Qing-zhu Yin

Received: 2 November 2012 / Accepted: 28 May 2013 / Published online: 27 June 2013

Abstract The nature of compositional heterogeneity within large silicic magma bodies has important implications for how silicic reservoirs are assembled and evolve through time. We examine compositional heterogeneity in the youngest (~170 to 70 ka) post-caldera volcanism at Yellowstone caldera, the Central Plateau Member (CPM) rhyolites, as a case study. We compare ^{238}U–^{230}Th age, trace-element, and Hf isotopic data from zircons, and major-element, Ba, and Pb isotopic data from sanidines hosted in two CPM rhyolites (Hayden Valley and Solfatara Plateau flows) and one extracaldera rhyolite (Gibbon River flow), all of which erupted near the caldera margin ca. 100 ka. The Hayden Valley flow hosts two zircon populations and one sanidine population that are consistent with residence in the CPM reservoir. The Gibbon River flow hosts one zircon population that is compositionally distinct from Hayden Valley flow zircons. The Solfatara Plateau flow contains multiple sanidine populations and all three zircon populations found in the Hayden Valley and Gibbon River flows, demonstrating that the Solfatara Plateau flow formed by mixing extracaldera magma with the margin of the CPM reservoir. This process highlights the dynamic nature of magmatic interactions at the margins of large silicic reservoirs. More generally, Hf isotopic data from the CPM zircons provide the first direct evidence for isotopically juvenile magmas contributing mass to the youngest post-caldera magmatic system and demonstrate that the sources contributing magma to the CPM reservoir were heterogeneous in $^{176}Hf/^{177}Hf$ at ca. 100 ka. Thus, the limited compositional variability of CPM glasses reflects homogenization occurring within the CPM reservoir, not a homogeneous source.

Keywords Yellowstone · Mixing · Zircon · Sanidine · ^{238}U–^{230}Th · Hf isotope

Introduction

Caldera volcanoes are typically associated with the largest explosive volcanic eruptions on Earth and pinpoint areas in the lithosphere where large volumes of mantle-derived magmas ascend and interact with their surroundings with the result of generating significant compositional diversity within the Earth's crust (e.g., Bachmann et al. 2007; Hildreth et al. 1991; White et al. 2006). The Yellowstone magmatic system is a prime example of a long-lived, large-volume silicic magma system that has produced numerous eruptions of rhyolite and basalt during Quaternary time. Yellowstone has generated three caldera-forming eruptions at 2.059 ± 0.004 Ma, 1.285 ± 0.004 Ma, and 0.639 ± 0.002 Ma (Lanphere et al. 2002), as well as numerous intracaldera and extracaldera eruptions between caldera-forming events (Christiansen 2001), and could potentially

Communicated by T L. Grove.

Electronic supplementary material The online version of this article (doi:10.1007/s00410-013-0893-2) contains supplementary material, which is available to authorized users.

M. E. Stelten (✉) · K. M. Cooper · G. H. Barfod · J. Wimpenny · Q. Yin
Department of Geology, University of California, Davis, Davis, CA, USA
e-mail: mestelten@ucdavis.edu

J. A. Vazquez
U.S. Geological Survey, Menlo Park, CA, USA

M. R. Reid
School of Earth Sciences and Environmental Sustainability, Northern Arizona University, Flagstaff, AZ, USA

be capable of further volcanic activity in the future (Christiansen et al. 2007; Girard and Stix 2012; Watts et al. 2012). A well-established volcanic stratigraphy makes Yellowstone a unique system for evaluating the time-compositional evolution of mafic and silicic magmas in an intracontinental hot spot setting (Christiansen 2001; Christiansen et al. 2007). The youngest phase of post-caldera volcanism within Yellowstone caldera generated the Central Plateau Member (CPM) of the Plateau Rhyolite in several episodes between ca. 170 and 70 ka (Christiansen et al. 2007), which serves as a time series that provides sequential snapshots into the geochemical evolution of the magmatic system over a ~100-ka interval. Previous studies establish that the reservoir of silicic magma that generated the CPM rhyolites evolved to cooler, more chemically evolved, and more isotopically juvenile compositions over time (Christiansen 2001; Girard and Stix 2010; Hildreth et al. 1991; Vazquez and Reid 2002; Vazquez et al. 2009; Watts et al. 2012). However, the physicochemical mechanisms that generate the chemical and isotopic diversity of silicic magmas at Yellowstone and the older calderas along the hot spot track remain uncertain, particularly the relative roles of deep- and shallow-level fractionation, contamination, and recycling in generating the isotopic and geochemical characteristics of small- and large-volume rhyolites (e.g., Bindeman et al. 2008; Boroughs et al. 2005; Hildreth et al. 1991; Leeman et al. 2008; McCurry and Rodgers 2009; Watts et al. 2010).

This paper provides new insight into the interaction of the Yellowstone magma reservoir with extracaldera magma and isotopically juvenile silicic magma ca. 100 ka by comparing ^{238}U–^{230}Th age, trace-element, and Hf isotopic data from individual zircons, and in situ major-element, Ba, and Pb isotopic data from sanidine hosted in two CPM rhyolites (the Solfatara Plateau flow and Hayden Valley flow), and one extracaldera rhyolite (the Gibbon River flow; zircon data only), all of which erupted near the northern margin of the caldera ca. 100 ka (Fig. 1). Linking ^{238}U–^{230}Th ages of zircons with their trace-element and isotopic compositions provides an effective approach for placing petrologic evolution within a framework of absolute time and for identifying the provenance (e.g., autocrysts versus antecrysts) of crystal populations (e.g., Bindeman et al. 2008; Carley et al. 2011; Claiborne et al. 2010a; Crowley et al. 2007; Klemetti et al. 2011; Reid et al. 2011; Schmitt 2006; Schoene et al. 2010; Schoene et al. 2012; Stelten and Cooper 2012; Watts et al. 2012). The Hf and oxygen isotopic composition of zircon provides a direct tracer of magmas with distinct sources that is insensitive to parameters such as temperature, oxygen fugacity, or the co-crystallizing assemblage (e.g., Kemp et al. 2007). Linking major-element compositions, Ba concentrations, and Pb isotopic compositions of individual sanidine crystals provides a robust method of identifying genetically distinct sanidine populations within and between rhyolites (e.g., Watts et al. 2012; Wolff and Ramos 2003) and allows us to track the crystallization history of the sanidines. The results of this multidimensional approach allow us to identify distinct crystal populations within the Solfatara Plateau flow (SPF) and Hayden Valley flow (HVF) and to place constraints on magma mixing at the margin of the CPM magma reservoir. Additionally, the zircon Hf isotope results yield the first direct evidence for the addition of isotopically juvenile rhyolite into Yellowstone caldera's post-collapse reservoir.

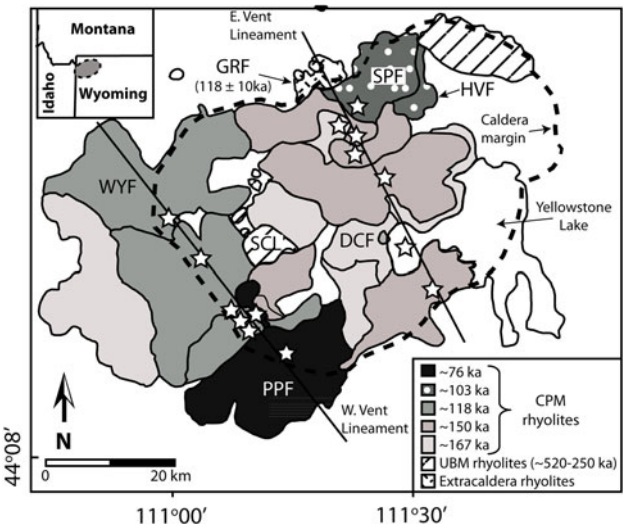

Fig. 1 Map of Yellowstone caldera, WY, showing the distribution of post-Lava Creek Tuff intracaldera and extracaldera lavas. Central Plateau Member (CPM) rhyolites have a *solid* or *dotted fill*, and the *shading* corresponds to the eruption age. Eruption ages of CPM rhyolites are lumped into five general groups following Christiansen et al. (2007). See Christiansen et al. (2007) for justification and the individual eruption ages. Vent locations are marked by white stars. The black dotted line is the caldera margin formed during the eruption of the Lava Creek Tuff at ca. 640 ka. Units for which zircon data are presented in this study are labeled. *DCF* Dry Creek flow, *GRF* Gibbon River flow, *HVF* Hayden Valley flow, *PPF* Pitchstone Plateau flow, *SCL* Scaup Lake flow, *SPF* Solfatara Plateau flow, *WYF* West Yellowstone flow. The *inset* shows the location of Yellowstone caldera in the western USA (*gray oval*). Map modified from Vazquez et al. (2009) after Christiansen (2001)

The post-caldera magmatic system at Yellowstone

General background

Post-collapse volcanism at Yellowstone caldera has been characterized by intermittent, dominantly effusive intracaldera (and volumetrically minor extracaldera) eruptions, which occurred in two broad episodes. The first episode erupted relatively small-volume lavas between 516 ± 7 ka

and 479 ± 10 ka (Gansecki et al. 1996) with two younger eruptions occurring ca. 260 ka (Bindeman et al. 2008; Christiansen et al. 2007) and collectively composed the Upper Basin Member of the Plateau Rhyolite. Upper Basin Member lavas are interpreted to represent individual magma batches generated by remelting of a low $\delta^{18}O$ protolith due to heat input from mafic magmas ponding beneath the magma reservoir and silicic recharge magmas injected into the reservoir, and perhaps with some assimilation of country rock (Bindeman et al. 2008; Christiansen et al. 2007; Gansecki et al. 1996; Girard and Stix 2009; Pritchard and Larson 2012; Watts et al. 2012).

After ca. 80 ka of quiescence, a second episode of post-collapse volcanism erupted 18 lavas and two ignimbrites between ca. 170 and 70 ka along two NNW-trending lineaments that are associated with major extracaldera faults (Christiansen 2001; Fig. 1). CPM rhyolites are voluminous with individual volumes of up to 70 km^3 (average ~10 km^3) and a collective volume of ~600 km^3 (Christiansen 2001; Christiansen et al. 2007). Age-correlated trends in (1) glass and whole-rock trace-element and isotopic compositions (Fig. 2a, b); (2) major-element compositions of major phases (Fig. 2c); and (3) geothermometry for CPM rhyolites suggest extraction from a common magma reservoir that progressively evolved to near-solidus temperatures, more fractionated compositions, higher $^{87}Sr/^{86}Sr$, and less radiogenic Pb isotopic compositions through a combination of fractional crystallization, assimilation, and magma recharge (Christiansen 2001; Girard and Stix 2010; Hildreth et al. 1984, 1991; Vazquez et al. 2009; Vazquez and Reid 2002; Watts et al. 2012).

Despite the largely coherent nature of CPM rhyolites erupted through time, there are some chemical distinctions between coeval rhyolites (Fig. 2a, b). We hereafter refer to CPM rhyolites that follow the general CPM trends with time as "main reservoir" CPM rhyolites (e.g., the Pitchstone Plateau flow, West Yellowstone flow, Hayden Valley flow, and Dry Creek flow), and any CPM rhyolites that lie off these trends as "anomalous" CPM rhyolites (e.g., the Solfatara Plateau flow; see Fig. 2). The large compositional distinctions between "main reservoir" and "anomalous" CPM rhyolites and the more subtle distinctions between coeval "main reservoir" CPM rhyolites in trace-element composition suggest some degree of heterogeneity in the magma reservoir despite the overall coherence of the trends (Fig. 2a, b; Girard and Stix 2010; Vazquez et al. 2009). Girard and Stix (2010) showed that slight differences in trace-element concentrations between coeval "main reservoir" CPM rhyolites erupted at ca. 160 ka can be correlated with their respective vent locations and suggested that rhyolites erupted from the eastern and western vent lineaments tapped different portions of a laterally extensive, yet incompletely mixed magma reservoir. Similarly, based on

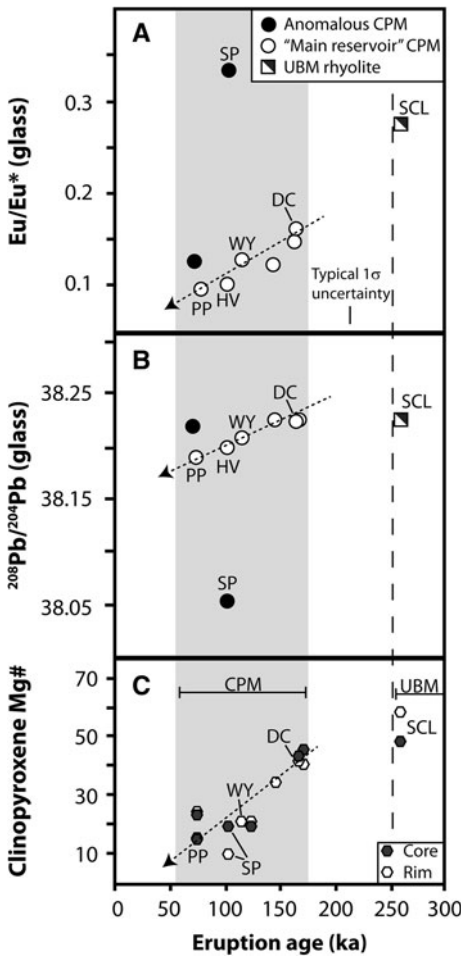

Fig. 2 Secular trends in glass and clinopyroxene composition through time. **a** Eu/Eu* (the europium anomaly) in erupted rhyolite glasses versus $^{40}Ar/^{39}Ar$ eruption age (ka). **b** $^{208}Pb/^{204}Pb$ of erupted rhyolite glasses versus $^{40}Ar/^{39}Ar$ eruption age. **c** Clinopyroxene Mg # versus $^{40}Ar/^{39}Ar$ eruption age. The *gray shaded* region represents the Central Plateau Member (CPM) eruptive episode. The *vertical dashed line* marks the end of the Upper Basin Member (UBM) eruptive episode. *Symbols* in **b** are the same as those in **a**. Unit labels are the same as in Fig. 1. Image modified from Vazquez et al. (2009). $^{40}Ar/^{39}Ar$ eruption ages are those reported in Christiansen et al. (2007). *Dashed arrows* show the "main reservoir" trends through time. Uncertainties on Pb isotopic measurements are smaller than the symbol size. Typical uncertainties on Eu/Eu* are included in the panel. Uncertainties on clinopyroxene Mg # are typically smaller than the symbol size. See Vazquez et al. (2009) for details on these data

zircon $\delta^{18}O$ compositions and sanidine Pb isotopic compositions, Watts et al. (2012) argued that the "main reservoir" CPM rhyolites preserve some evidence for compositional heterogeneity early in the CPM episode, but progressively become more homogeneous throughout the eruptive episode. The origin of "anomalous" CPM rhyolites is poorly understood and has been attributed to mixing or assimilation of older rhyolites within the reservoir (Vazquez et al. 2009). Thus, the "anomalous" CPM rhyolites are key end-members for understanding the relative

roles of magma mixing and recharge that are otherwise obscured by geochemical homogenization within the reservoir.

The Hayden Valley, Solfatara Plateau, and Gibbon River flows

The HVF is a "main reservoir" CPM rhyolite with a volume of $\sim$2 km^3 that erupted from the eastern vent lineament near the northern margin of the caldera (Fig. 1; Christiansen et al. 2007; Vazquez et al. 2009; Vazquez and Reid 2002). The SPF is a compositionally "anomalous" CPM rhyolite with a volume of $\sim$7 km^3 that vented adjacent to the HVF (Fig. 1; Christiansen et al. 2007). The SPF and HVF yield mutually indistinguishable ^{40}Ar/^{39}Ar ages of 102 $\pm$ 4 ka and 103 $\pm$ 8 ka (Christiansen et al. 2007), respectively, with stratigraphic relations indicating that SPF is the younger of the two lavas (Christiansen 2001). The "anomalous" composition of the SPF is manifested by a unique trace-element composition (higher Ba, Sr, Eu/Eu*, Hf; lower U, Th, Rb) and isotopic composition (Pb, O, Sr) relative to all other CPM rhyolites (Fig. 2; Bindeman and Valley 2001; Vazquez and Reid 2002; Vazquez et al. 2009). Chemical zoning in clinopyroxene and quartz from the SPF is consistent with late-stage mixing within the SPF magma prior to eruption (Fig. 2c; Vazquez et al. 2009). Despite these geochemical and isotopic distinctions between the SPF and "main reservoir" CPM rhyolites, ^{238}U–^{230}Th age data document coeval zircon crystallization in the SPF and "main reservoir" CPM rhyolites erupted from 166 to 114 ka (Vazquez and Reid 2002; Watts et al. 2012). Primarily based on Nd–Pb isotopic relations, the older (ca. 515–470 ka) Upper Basin Member rhyolites and Lava Creek Tuff can be ruled out as remelted sources or mixing end-members involved in the origin of the SPF (Vazquez et al. 2009). However, the anomalous composition of the SPF rhyolite glass could be due to late-stage mixing of a "main reservoir" CPM rhyolite with remelted hydrothermally altered Huckleberry Ridge Tuff left over from the caldera-forming eruption at $\sim$2.1 Ma (Vazquez et al. 2009). Alternatively, the end-members involved in the mixing could represent batches of post-collapse rhyolite that ascended to shallow levels but were not directly sampled by volcanic eruptions (e.g., Tappa et al. 2011).

In this context, it is noteworthy that Girard and Stix (2010) present trace-element concentrations for SPF and HVF samples that are the opposite of those presented by Vazquez et al. (2009) and Bindeman and Valley (2001), i.e., a reversal of "main reservoir" versus "anomalous" distinctions for these two flows. Girard and Stix (2010) suggested that this discrepancy could indicate that the HVF and SPF represent compositionally bimodal lava flows formed when two compositionally distinct lavas erupted during a single event, or when a single compositionally complex magma reservoir was erupted. Alternatively, this observation may signal imprecision in the mapped field relations between these overlapping and partly buried lavas (cf. Christiansen 2001). However, the important aspect of the SPF and HVF rhyolites is the close association of two geochemically distinct compositions of silicic magma in time and space, and not whether these compositions effused as one or two separate lavas. Accordingly, the conclusions regarding compositional heterogeneity at the margin of the Yellowstone reservoir are relevant to the compositions of magma that interact in the subsurface and are independent of the details of eruption history. In this paper, we treat the HVF as the rhyolite with "main reservoir" characteristics and the SPF as the rhyolite with "anomalous" characteristics, because the samples used in this study are the same samples used in Vazquez and Reid (2002) and Vazquez et al. (2009). This distinction allows us to directly compare the results presented in this paper with those presented by Vazquez and Reid (2002) and Vazquez et al. (2009).

The GRF is an extracaldera rhyolite that erupted at 118 $\pm$ 10 ka (Christiansen et al. 2007) immediately adjacent to the SPF and HVF. The GRF and other extracaldera rhyolites are thought to be crustal melts that are unrelated to main reservoir magmatism due to their distinct trace-element and isotopic (Pb, O, Sr, Nd) compositions compared to "main reservoir" CPM rhyolites (Hildreth et al. 1991). GRF zircons yield a younger average age ($\sim$140 ka) than zircons hosted in CPM rhyolites erupted from ca. 165 to 100 ka, but with significant overlap in their zircon model age distributions.

Sampling and methods

All glass, zircon, and sanidine in this study were separated from the same rhyolite lava samples used in Vazquez and Reid (2002) and Vazquez et al. (2009). Thus, the data presented here are directly comparable to the data from those studies. See Vazquez and Reid (2002) for sample descriptions.

Electron microprobe analyses

Forty-seven sanidine grains from the SPF and 29 grains from the HVF were analyzed for major-element and Ba concentrations on the Cameca SX 100 electron microprobe (EMP) in the Department of Geology at UC Davis. All sanidine grains were analyzed in situ in thick mounts and were imaged in backscattered electron mode and cathodoluminescence mode prior to analysis to guide the

location of the analysis spots and to document textural context. Multiple analyses were performed on each sanidine grain to characterize core to rim chemical zoning. Run conditions and the full data set are presented in Online Resource C1.

Pb isotopic analyses

A subset of sanidine grains from the SPF (15 grains) and HVF (9 grains) previously analyzed for major-element and Ba concentrations by EMP were analyzed for Pb isotopic compositions by laser ablation multiple-collector inductively coupled plasma mass spectrometry (LA-MC-ICPMS) following the method of Kent (2008). We also measured the Pb isotopic compositions of the groundmass glasses in which the HVF and SPF sanidines are hosted (i.e., from the same thick mount). All analyses were conducted using a Nu Plasma MC-ICPMS coupled with a 213-nm laser ablation system housed in the Interdisciplinary Center for Plasma Mass Spectrometry at UC Davis. LA-MC-ICPMS analyses on sanidine crystals were conducted after EMP analyses, and LA-MC-ICPMS analysis spots were located directly on the top of the previous EMP spots (or adjacent to EMP spots but in the same zone of the crystal based on cathodoluminescence imaging). See Online Resource A1 for details on the analytical method, operating conditions, and data reduction.

Zircon ^{238}U–^{230}Th dating and trace-element analyses

Zircon grains separated from each sample were mounted in epoxy, ground to near the center of the grains, and polished prior to analysis. Due to variation in the size of the zircon grains on a given mount, this grinding/polishing procedure will reveal different depths within the zircon for different-sized grains. Thus, the center of each cross-sectional surface exposed in the zircons may not be the "true" core of the grain. For all grains, reflected light and cathodoluminescence images were obtained prior to analysis and used to guide the location of the analyses. Zircons from the Pitchstone Plateau flow, West Yellowstone flow, Dry Creek flow, SPF, GRF, and the ca. 260 ka Upper Basin Member Scaup Lake flow that were used for U–Th and U–Pb dating by Vazquez and Reid (2002; Scaup Lake flow zircon U–Pb ages were not published) were re-analyzed for trace-element concentrations using a CAMECA ims 1270 ion microprobe at UCLA following the protocol and standardization described in Schmitt and Vazquez (2006) and Reid et al. (2011). Additional zircons were separated from the original samples of the HVF and SPF and analyzed for ^{238}U–^{230}Th ages and trace-element concentrations using the Stanford-USGS SHRIMP-RG ion microprobe. The instrument used for age and trace-element analyses for each grain is given in Online Resource C2, and analytical details are described in Online Resource A1. Trace-element analyses were performed first, followed by ^{238}U–^{230}Th dating in the same locations. A subset of SPF and GRF zircons were analyzed at both UCLA and Stanford for trace-element concentrations, and the results indicate that no significant bias between the data sets was generated using different instruments and standards (Online Resource A1).

Zircon oxygen isotopic analyses

A subset of SPF and GRF zircons were analyzed for oxygen isotopic compositions using a CAMECA ims 1270 ion microprobe at UCLA, following the methods described in Trail et al. (2007). Oxygen isotopic analyses were conducted after ^{238}U–^{230}Th age analyses and trace-element analyses, but prior to Hf isotopic analyses. The zircon mounts were lightly ground and polished prior to the analytical session to remove any implanted oxygen from previous SIMS analyses and to produce a flat surface for analysis. Oxygen isotope analyses were located directly below previous ^{238}U–^{230}Th ages and trace-element analyses. Instrumental mass fractionation was determined from repeated analysis of 91500 zircon standard ($\delta^{18}O = 9.9$ ‰; Wiedenbeck et al. 2004). The external uncertainty from repeated analysis of 91500 during the analytical session is 0.23 ‰ (1 SD).

Zircon LA-MC-ICPMS Hf isotopic analyses

Zircons from the HVF, SPF, and GRF analyzed for ^{238}U–^{230}Th ages and trace-element concentrations were analyzed for Hf isotopic compositions by LA-MC-ICPMS at the University of California, Davis, using a 193-nm excimer laser coupled with a Neptune Plus MC-ICPMS. LA-MC-ICPMS spots were analyzed last and co-located with age and trace-element spots. LA-MC-ICPMS analyses were performed using a ~53 μm diameter spot size, 8 Hz pulse rate, and 25 % laser energy. Pit depths under these conditions are estimated to be ~25 μm (Tollstrup et al. 2012). See Online Resource A1 for details on standard analyses and data reduction.

MC-ICPMS Hf isotopic analysis of glass and whole rock

Approximately 50–100 mg of glass from the HVF, SPF, West Yellowstone flow, Pitchstone Plateau flow, and Dry Creek flow was isolated and purified by magnetic separation, and visual selection using a petrographic microscope. For the GRF, bulk sample was crushed to a fine powder and ~100 mg of powder was used for Hf isotopic analysis. Hf

was separated from the CPM glasses and GRF whole rock using dissolution procedures and ion-exchange chromatography as described in Online Resource A2. Hf isotopic analyses on the CPM glasses were performed on a Neptune Plus MC-ICPMS at UC Davis, whereas analysis of the GRF sample was performed on a Nu Plasma MC-ICMPS in the Interdisciplinary Center for Plasma Mass Spectrometry at UC Davis. Analytical techniques, standard and blank analyses, and analytical errors are discussed in Online Resource A2.

Kolmogorov–Smirnov statistical tests

To evaluate the zircon age data and test whether the age distributions of different zircon populations are statistically distinct, we performed a series of two-sample Kolmogorov–Smirnov (KS) tests comparing distributions of zircon-glass ^{238}U–^{230}Th isochron slopes between different zircon populations (see Storm et al. 2011 and Schmitt 2011 for other examples of this approach). The KS test compares the empirical distribution functions of two samples and tests the null hypothesis that the two samples are drawn from the same underlying distribution. We use isochron slopes instead of ages because the uncertainties of the isochron slopes are symmetric about the mean, unlike the U–Th model ages. However, the KS test does not account for analytical uncertainties in the data; therefore, we used a Monte Carlo approach to assess the robustness of the KS test results to measurement uncertainties. In this Monte Carlo simulation, we assume that the uncertainty of the isochron slope for each analysis is normally distributed about its mean. For each of 50,000 iterations, we randomly perturb the isochron slope for each zircon ^{238}U–^{230}Th analysis within its analytical uncertainty in the data sets being compared and perform KS tests on the perturbed isochron slopes. We then calculate the percentage of the KS tests that reject the null hypothesis for each simulation. The results of the KS tests and Monte Carlo approach to estimate uncertainties are discussed in "The origin of young zircon populations at Yellowstone."

Results

Electron microprobe analyses

Major-element and Ba concentrations of sanidine measured by EMP are presented in Fig. 3 and Online Resource C1. Sanidines from the HVF have a limited range of major-element composition, with X_{Or} ranging from 38.2 to 53.2 and an average of 50.6 ± 4.4 (2σ), although the majority (92 %) of sanidine analyses have X_{Or} between 49 and 53. Ba concentrations of HVF sanidines range from 878 to 3,242 ppm, with an average of 1,637 ± 874 ppm (2σ). Sanidines from the SPF display more heterogeneity in major-element composition, with X_{Or} ranging from 19.7 to 46.9 and an average of 41.9 ± 8.5 (2σ), although the majority (77 %) of sanidine analyses have X_{Or} between 40 and 47. Additionally, SPF sanidines have a wide range of Ba concentration from 1,600 to 10,900 ppm, with a mean of 6,082 ± 4,055 ppm (2σ). Ba does not correlate with X_{Or} for sanidine in either flow (Fig. 3).

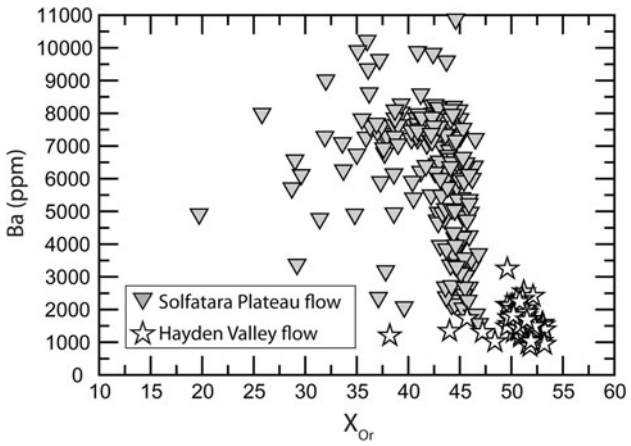

Fig. 3 Ba (ppm) versus X_{Or} for Solfatara Plateau flow and Hayden Valley flow sanidine crystals. *Each data point* is an electron microprobe analysis of a 10-μm-diameter zone within a sanidine grain. Note that the sanidines from the SPF and HVF have distinct compositions. Also note the restricted range of composition of HVF sanidines relative to the SPF sanidines

Pb isotopic data

Pb isotopic compositions measured for HVF and SPF sanidines and glasses are reported in Fig. 4 and Online Resource C1. Pb isotopic compositions of HVF and SPF glasses measured by LA-MC-ICPMS in this study agree well with Pb isotopic compositions of HVF and SPF glasses measured by Vazquez et al. (2009) via solution MC-ICPMS (Fig. 4 and Online Resource C1). The HVF glass is characterized by lower $^{208}Pb/^{206}Pb$ and $^{207}Pb/^{206}Pb$ but higher $^{208}Pb/^{204}Pb$, $^{207}Pb/^{204}Pb$, and $^{206}Pb/^{204}Pb$ compared to the SPF glass. All HVF sanidines have homogeneous Pb isotopic compositions that are indistinguishable from each other and the host HVF glass when considering the 2σ uncertainty on each analysis (Fig. 4). No HVF sanidines show intragrain Pb isotopic zoning outside of the reported 2σ uncertainty. On the other hand, SPF sanidines display a relatively wide range of Pb isotopic compositions, especially with regard to $^{208}Pb/^{206}Pb$ and $^{207}Pb/^{206}Pb$, and are isotopically distinct from HVF sanidine (Fig. 4). The majority of SPF sanidines have Pb isotopic compositions within error of the host SPF glass at the 2σ level, but a significant number of sanidines have Pb isotopic

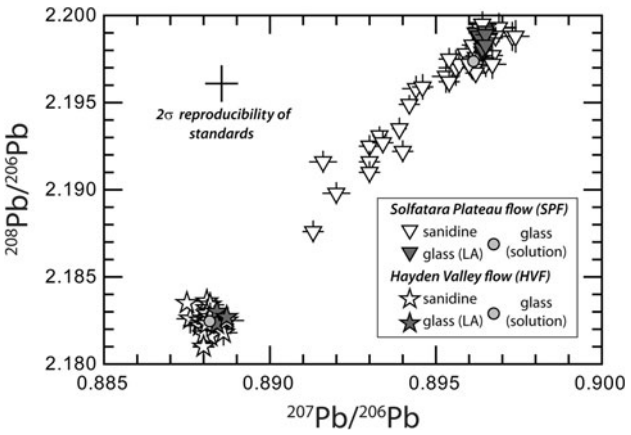

Fig. 4 $^{208}Pb/^{206}Pb$ versus $^{207}Pb/^{206}Pb$ for Hayden Valley flow and Solfatara Plateau flow sanidines and glass. All sanidine Pb isotopic compositions were measured via LA-MC-ICPMS. Glass (LA) represents the glass compositions measured via LA-MC-ICPMS in this study. Glass (solution) represents the glass compositions measured via solution MC-ICPMS by Vazquez et al. (2009) for the same samples used in this study. Note the distinct Pb isotopic compositions of the HVF and SPF sanidines and glass. HVF sanidines have a very restricted range of Pb isotopic composition that is within error of the host glass (i.e., host melt) and show no evidence of isotopic heterogeneity. On the other hand, SPF sanidines show a wide range of Pb isotopic composition and preserve abundant evidence for isotopic heterogeneity. Most analyses of SPF sanidines are within error of the host glass, but a subset of analyses extends to lower $^{208}Pb/^{206}Pb$ and $^{207}Pb/^{206}Pb$ values that are more similar to the HVF glass and sanidines. Also note the excellent agreement between solution MC-ICPMS and laser ablation MC-ICPMS values for glasses. Uncertainties shown with the data points are 1 SE analytical uncertainty. The reproducibility (2 standard deviations) of the external check standard (NIST 612) for laser ablation analyses is included in the *upper left-hand corner*

compositions that extend to $^{208}Pb/^{206}Pb$ and $^{207}Pb/^{206}Pb$ values that are intermediate between the SPF and HVF glasses.

Zircon trace-element concentrations and ^{238}U–^{230}Th ages

New ^{238}U–^{230}Th ages of zircons from the SPF and HVF, as well as ages previously reported by Vazquez and Reid (2002) for SPF, GRF, Pitchstone Plateau flow, West Yellowstone flow, and Dry Creek flow zircons are summarized in Table 1, and full data are reported in Online Resource C2. Model ^{238}U–^{230}Th ages from zircon (Reid et al. 1997) were calculated assuming that the zircons crystallized from and remained in isotopic equilibrium with their host melt (i.e., surrounding groundmass glass). Because no U-series data exist for the HVF glass, model ages for HVF zircons are calculated using the glass composition of the Pitchstone Plateau flow. This is justified because U and Th isotopic compositions of other CPM rhyolite glasses are similar to the Pitchstone Plateau flow glass (Vazquez and Reid 2002), suggesting restricted U–Th isotopic compositions in the Yellowstone magma reservoir. Additionally, we include a 20 % uncertainty in the glass composition when calculating zircon ages, which encompasses the variation in $(^{238}U)/(^{232}Th)$ and $(^{230}Th)/(^{232}Th)$ observed for intracaldera CPM rhyolites and extracaldera GRF combined ($\sim$15 %; Vazquez and Reid 2002).

New ^{238}U–^{230}Th model ages for SPF zircons dominantly fall between ca. 130 and 200 ka (although three crystals are within error of secular equilibrium) and are indistinguishable from the range of single crystal model ages reported by Vazquez and Reid (2002). Similar to SPF zircons, the ^{238}U–^{230}Th ages for HVF zircons range from ca. 118 ka to within error of secular equilibrium. However, the HVF has proportionally more zircons that are within error of secular equilibrium when compared to the SPF (Fig. 5). Given the small sample size for zircon ^{238}U–^{230}Th ages, it is unclear whether or not the larger proportion of zircons within error of secular equilibrium in the HVF reflects a real difference in the age of the zircon populations.

Complete trace-element data for zircons from the SPF, HVF, GRF, Pitchstone Plateau flow, West Yellowstone flow, Dry Creek flow, and Scaup Lake flow are reported in Online Resource C2, and selected trace-element data are reported in Table 1. In general, zircons from "main reservoir" CPM rhyolites (i.e., Pitchstone Plateau flow, West Yellowstone flow, and Dry Creek flow) have distinct trace- and minor-element characteristics when compared to zircons from the extracaldera GRF and the older Scaup Lake flow. For example, zircons from "main reservoir" CPM rhyolites have higher Hf concentrations and lower Eu/Eu* compared to GRF zircons (Fig. 6a). Although we focus here on Hf concentrations and Eu/Eu*, the geochemical distinctions between GRF and "main reservoir" CPM zircons are robust because these zircon populations can be distinguished using many elements (and element ratios) including P, Ti, Y, U, Th, and any HREE (Online Resource B1). Zircons from the Upper Basin Member Scaup Lake flow define a field that partially overlaps the CPM field in Fig. 6a, but is characterized by a wider range of Eu/Eu* and higher Hf concentrations. These Scaup Lake flow zircons form poorly defined fields in most trace-element plots and for some elements (e.g., Eu/Eu* vs. Hf and Y/U vs. P) are more similar to "main reservoir" CPM zircons, while they are more similar to GRF zircons in other elements (e.g., Lu vs. Eu and U + Th vs. Ti; Online Resource B1).

Zircons from the HVF dominantly lie within the "main reservoir" CPM field except for a few analyses lying in the GRF and Scaup Lake flow fields, and one analysis with very high Hf ($\sim$ 14,300 ppm) that does not lie in any of the defined fields (Fig. 6b). Zircons from the SPF span a relatively wide range of compositions with roughly equal proportions of zircons within the "main reservoir" CPM

Table 1 Model ages, Hf isotopic data, oxygen isotopic data, and selected trace-element data for Yellowstone zircons

Analysis name	Zircon pop.	Hf (ppm)	Eu/Eu*	(^{230}Th)/(^{232}Th)	±1σ	(^{238}U)/(^{232}Th)	± 1σ	Age (ka)	+ 1σ	− 1σ	ε_{Hf}	± 2σ	δ^{18}O (‰)
Gibbon River flow													
GRF_R3_G1_S1C	N/A	7,761	0.28	4.11	0.43	4.8	0.06	183	107	52	−5.5	0.9	3.09
GRF_R3_G1_S2C	N/A			3.29	0.26	4.21	0.01	139	34	26			2.98
GRF_R3_G1_S3R	N/A										−6.6	0.9	2.17
GRF_R3_G2_S1M	N/A										−6.7	0.9	3.33
GRF_R3_G2_S2C	N/A			3.2	0.45	4.92	0.01	94	32	25	−5.7	0.9	3.38
GRF_R3_G2_S3R	N/A										−7.0	0.9	
GRF_R3_G4_S1C	N/A			3.7	0.21	4.86	0.01	133	21	18	−9.2	0.9	5.12
GRF_R3_G4_S2C-R	N/A										−8.0	0.9	2.92
GRF_R3_G4_S3R	N/A										−6.9	0.9	
GRF_R3_G4_S4R	N/A										−6.9	0.9	
GRF_R3_G5_S1C	N/A			4.11	0.25	4.92	0.02	171	40	29	−7.8	0.9	2.78
GRF_R3_G5_S2R	N/A										−6.3	0.9	3.34
GRF_R3_G5_S3C-M	N/A										−7.3	0.9	
GRF_R3_G5_S4R	N/A										−5.6	0.9	
GRF_R3_G6_S1C	N/A			4.92	0.22	6.16	0.02	156	22	18	−6.0	0.9	2.98
GRF_R3_G6_S2C-R	N/A										−5.6	0.9	
GRF_R3_G7_S1C	N/A										−7.6	0.9	2.54
GRF_R3_G7_S2C	N/A	9,923	0.18	2.78	0.12	3.68	0.07	123	21	17	−8.3	0.9	2.06
GRF_R3_G7_S3R	N/A	8,523	0.13	4.57	0.37	6.48	0.02	117	24	19	−6.6	0.9	
GRF_R3_G7_S4	N/A	9,793	0.16										
GRF_R3_G9_S2C	N/A	9,099	0.14	3.33	0.26	4.72	0.02	112	23	19	−6.4	0.9	3.29
GRF_R3_G9_S1R	N/A	9,060	0.11	3.83	0.32	5.81	0.02	101	19	16	−7.3	0.9	2.10
GRF_R3_G9_S3R	N/A										−7.1	0.9	
GRF_R3_G9_S4 M	N/A										−5.6	0.9	
GRF_R4_G10_S1C	N/A			5.22	0.23	6.81	0.02	143	17	15	−6.0	0.9	3.16
GRF_R4_G10_S2R	N/A										−6.0	0.9	
GRF_R5_G9_S1 M	N/A										−5.5	0.9	
GRF_R5_G9_S2 M-R	N/A												
GRF_R5_G9_S3C	N/A												
GRF_R5_G9_S4R	N/A												
GRF_R5_G10_S1C-M	N/A										−5.6	0.9	
GRF_R5_G13_S1C	N/A										−7.3	0.9	2.55
GRF_R5_G13_S2R	N/A										−5.8	0.9	
GRF_R6_G12_S1C-M	N/A			4.2	0.44	5.6	0.33	132	73	39			3.14
GRF_R6_G12_S2 M-R	N/A										−7.0	0.9	
GRF_R4_G2_S1C	N/A	7,642	0.23	4.53	0.43	5.92	0.1	140	47	32	−6.5	0.9	2.98
GRF_R4_G2_S2 M	N/A										−6.6	0.9	3.53
GRF_R4_G2_S3 M-C	N/A										−6.4	0.9	2.81
GRF_R4_G2_S4R	N/A	8,707	0.22	4.85	0.46	6.57	0.02	130	34	25			
Hayden Valley flow													
HV-G27-S1C	Inherited	11,903	0.14	3.78	0.33	3.88	0.06	351	–	155	−5.7	1.9	
HV-G27-S2R	Inherited	11,913	0.08								−7.0	1.9	
HV-G25-S1	?												
HV-G24-S1	?										−3.6	1.9	
HV-G22-S1	?										−5.7	1.9	
HV-G17-S1C	MR-like	11,468	0.11	4.13	0.38	4.33	0.06	302	–	118	−2.6	1.9	
HV-G17-S2R	MR-like	11,366	0.08								−6.0	1.9	

Table 1 continued

Analysis name	Zircon pop.	Hf (ppm)	Eu/Eu*	(^{230}Th)/(^{232}Th)	±1σ	(^{238}U)/(^{232}Th)	± 1σ	Age (ka)	+ 1σ	− 1σ	ε_{Hf}	± 2σ	$\delta^{18}O$ (‰)
HV-G17-S3 M	MR-like												
HV-G16-S1R	Inherited	11,151	0.08								−7.3	1.9	
HV-G16-S2 M	Inherited	11,835	0.16								−4.4	1.9	
HV-G16-S3C	Inherited	11,548	0.06	3.19	0.24	3.80	0.05	171	73	43			
HV-G15-S1C	Inherited	11,893	0.13	4.46	0.42	4.77	0.07	270	–	95	−4.9	1.9	
HV-G15-S2R	Inherited	11,555	0.06								−6.0	1.9	
HV-G14-S1C	MR-like	11,250	0.05	3.91	0.34	4.33	0.06	228	244	70	−4.2	1.9	
HV-G14-S2R	MR-like	11,447	0.08								−5.6	1.9	
HV-G12-S1C	MR-like	11,668	0.06	3.72	0.33	4.88	0.07	136	43	31	−2.5	1.9	
HV-G12-S2R	MR-like	10,228	0.13								−4.3	1.9	
HV-G10-S1C	MR-like	11,362	0.12	4.63	0.45	4.57	0.07	–	–	–	−2.3	1.9	
HV-G10-S2R	MR-like	11,439	0.08								−5.2	1.9	
HV-G4-S1C	MR-like	11,940	0.06	4.25	0.39	4.58	0.07	262	–	90			
HV-G4S2R	MR-like	11,277	0.07								−5.5	1.9	
HV-G3-S1C	Pop. 5	14,280	0.01	4.55	0.33	6.50	0.09	117	23	19	−5.1	1.9	
HV-G3-S2R	Pop. 5	11,395	0.07										
HV-G1-S1C	Mixed	8,074	0.18								1.2	1.9	
HV-G1-S2R	Mixed	10,425	0.12								−3.5	1.9	
HV-G1-S3C	Mixed	8,402	0.15								−1.4	1.9	
HV-G1-S5C	Mixed										−0.9	1.9	
Solfatara Plateau flow													
SP(A)_R7_G2_S1C-M	Mixed	10,569	0.15	5.34	0.4	6.33	0.02	188	59	38	−6.3	0.9	2.79
SP(A)_R7_G2_S2C-M	Mixed	8,411	0.18								−6.2	0.9	3.02
SP(A)_R8_G1_S2C	EC-like	8,321	0.32	3.77	0.27	5	0.06	134	33	25	−6.8	0.9	2.04
SP(A)_R8_G1_S1R	EC-like	8,384	0.25	5.33	0.46	6.93	0.03	146	39	28	−8.4	0.9	2.35
SP(A)_R8_G1_S3	EC-like	8,100	0.29								−6.8	0.9	2.35
SP(A)_R8_G1_S4	EC-like	9,482	0.19								−6.8	0.9	2.35
SP(A)_R8_G2_S2C	Mixed	9,623	0.20								−5.8	0.9	3.37
SP(A)_R8_G2_S3	Mixed	10,251	0.19								−5.3	0.9	3.28
SP(A)_R8_G3_S1 M-R	MR-like	10,508	0.06	4.85	0.62	5.42	0.02	226	–	79	−6.8	0.9	3.42
SP(A)_R8_G3_S2 M-C	MR-like	11,091	0.08								−6.5	0.9	3.18
SP(A)_R8_G3_S3	MR-like	11,394	0.08								−6.8	0.9	
SP(A)_R8_G5_S1R	MR-like	9,947	0.06								−6.1	0.9	4.17
SP(A)_R8_G5_S2C	MR-like	10,920	0.06	4.74	0.36	6.06	0.14	150	48	32	−6.7	0.9	3.87
SP(A)_R8_G5_S3C-M	MR-like	11,308	0.10								−6.6	0.9	
SP(A)_R8_G5_S4	MR-like	11,581	0.06								−6.7	0.9	3.87
SP(A)_R8_G6_S1C-R	MR-like			4.52	0.21	5.61	0.02	162	25	20	−7.3	0.9	3.25
SP(A)_R8_G6_S2C	MR-like	12,267	0.07								−7.4	0.9	3.31
SP(A)_R8_G6_S3R	MR-like	11,657	0.08								−6.1	0.9	
SP(A)_R8_G7_S1 M-R	?			2.39	0.03	2.8	0.00	171	10	9			2.79
SP(A)_R8_G7_S2C	?												3.00
SP(A)_R8_G7_S3 M-R	Inherited	12,123	0.03										2.99
SP(A)_R8_G8_S1C-M	EC-like	8,871	0.19	4.62	0.23	5.83	0.02	155	25	20	−5.8	0.9	2.76
SP(A)_R8_G8_S2C	EC-like	9,480	0.21								−6.0	0.9	2.88
SP(A)_R8_G8_S3R	EC-like										−6.5	0.9	
SP(A)_R8_G9_S1C	Inherited	10,658	0.08	3.85	0.18	3.95	0.01	359	–	104	−4.7	0.9	3.07
SP(A)_R8_G9_S2R	Inherited	12,455	0.08										
SP(A)_R8_G9_S3	Inherited	13,073	0.11										

Table 1 continued

Analysis name	Zircon pop.	Hf (ppm)	Eu/Eu*	(^{230}Th)/(^{232}Th)	±1σ	(^{238}U)/(^{232}Th)	± 1σ	Age (ka)	+ 1σ	− 1σ	ε_{Hf}	± 2σ	$\delta^{18}O$ (‰)
SP(A)_R8_G9_S4	Inherited	11,581	0.07								−6.9	0.9	
SP(A)_R8_G10_S1C-M	MR-like	10,760	0.08	4.36	0.13	5.3	0.02	171	18	16	−6.5	0.9	3.21
SP(A)_R8_G10_S2	MR-like	11,804	0.10										
SP(A)_R8_G10_S3	MR-like	10,701	0.08								−6.5	0.9	
SP(A)_R9_G8_S1C	MR-like	11,189	0.09	4.09	0.13	4.72	0.02	199	30	23	−5.6	0.9	3.35
SP(A)_R9_G8_S2 M	MR-like	11,267	0.06								−7.1	0.9	2.84
SP(A)_R9_G8_S3C	MR-like	11,334	0.07								−5.0	0.9	
SP(A)_R9_G4_S1 M-R	EC-like	9,271	0.23	3.96	0.32	5.12	0.02	143	37	27	−6.8	0.9	2.40
SP(A)_R9_G4_S2C	EC-like	8,461	0.19								−5.7	0.9	3.48
SP(A)_R9_G4_S3	EC-like	9,589	0.26										
SP(A)_R9_G2_S1 M	EC-like	8,184	0.28	4.08	0.27	5.79	0.02	117	20	17	−5.5	0.9	1.67
SP(A)_R9_G2_S2C	EC-like	8,886	0.15								−5.1	0.9	3.09
SP(A)_R9_G2_S3 M	EC-like	8,826	0.22								−6.0	0.9	
SP(A)_R9_G2_S4	EC-like	9,230	0.26								−5.5	0.9	1.67
SP(A)_R9_G1_S2C	Mixed	9,376	0.17	6.05	0.63	7.18	0.03	188	93	49	−5.4	0.9	3.56
SP(A)_R9_G1_S3R	Mixed	10,006	0.13	6.05	0.63	7.18	0.03	188	93	49	−7.3	0.9	2.96
SP(A)_R9_G1_S1C	Mixed	12,224	0.07										
SP-G1-S1C	MR-like	11,500	0.12	4.42	0.42	5.11	0.07	199	120	56	−0.5	1.9	
SP-G1-S2R	MR-like	11,523	0.06								0.2	1.9	
SP-G2-S1C	Mixed	10,608	0.06	3.98	0.38	5.06	0.07	149	54	36			
SP-G2-S2R	Mixed	9,599	0.15										
SP-G8-S1C	EC-like	8,675	0.23										
SP-G8-S2R	EC-like	9,500	0.16										
SP-G8-S3C	EC-like												
SP-G9-S1C	Mixed	10,122	0.13								−2.2	1.9	
SP-G9-S2R	Mixed	9,567	0.18								−3.0	1.9	
SP-G10-S1	?										0.4	1.9	
SP-G11-S1C	Mixed	10,899	0.14	4.05	0.35	4.06	0.06	540	–	319			
SP-G11-S2R	Mixed	10,189	0.14								−5.3	1.9	
SP-G12-S1C	Mixed	11,275	0.06	3.86	0.35	4.88	0.07	151	53	36	−2.6	1.9	
SP-G12-S2R	Mixed	9,550	0.15								−3.9	1.9	
SP-G14-S1C	Mixed	10,797	0.06	3.95	0.40	5.10	0.07	144	52	35	−3.9	1.9	
SP-G14-S2R	Mixed	10,036	0.14								−3.9	1.9	
SP-G15-S1C	MR-like	11,293	0.07	4.11	0.37	4.90	0.07	179	81	46	−1.9	1.9	
SP-G15-S2R	MR-like	11,224	0.06								−6.0	1.9	
SP-G16-S1C	Inherited	11,644	0.14	1.56	0.15	1.59	0.02	314	–	202	−4.1	1.9	
SP-G16-S3R	Inherited	11,283	0.10								−6.3	1.9	
SP-G16-S2C	Inherited			4.50	0.41	4.62	0.07	361	–	159			
SP-G17-S4C	Mixed	12,008	0.07	3.18	0.25	4.13	0.06	137	43	31	−1.2	1.9	
SP-G17-S5R	Mixed	9,177	0.19								−5.8	1.9	
SP-G17-S2 M	Mixed	11,968	0.09								−3.4	1.9	
SP-G17-S3R	Mixed										−4.1	1.9	
SP-G17-S4R	Mixed										−5.1	1.9	
SP-G20-S2R	MR-like	11,309	0.08								−2.9	1.9	
SP-G20-S3C	MR-like	11,400	0.08	3.44	0.29	4.24	0.06	159	60	39			
SP-G22-S1C	Mixed	9,036	0.16	3.18	0.43	4.25	0.06	128	61	39			
SP-G22-S3R	Mixed	10,465	0.18								−5.2	1.9	
SP-G22-S2 M	Mixed	8,857	0.28										

Table 1 continued

Analysis name	Zircon pop.	Hf (ppm)	Eu/Eu*	(^{230}Th)/(^{232}Th)	±1σ	(^{238}U)/(^{232}Th)	± 1σ	Age (ka)	+ 1σ	− 1σ	ε_{Hf}	± 2σ	δ^{18}O (‰)
Dry Creek flow													
YCV14r4g2s1	N/A	11,013	0.08	2.79	0.14	3.46	0.07	149	36	26			
YCV14r4g3s1	N/A	10,886	0.10	3.42	0.18	4.07	0.02	175	38	28			
YCV14r4g4s1	N/A	10,333	0.13	3.72	0.33	4.62	0.02	157	53	35			
YCV14r5g5s1	N/A	10,498	0.09	3.00	0.2	3.84	0.01	139	31	24			
YCV14r6g2s1	N/A	11,409	0.05	4.55	0.28	4.82	0.01	288	–	76			
YCV14r6g2s4	N/A	11,343	0.12										
YCV14r6g3s1	N/A	10,974	0.10	3.00	0.22	3.43	0.04	193	91	48			
YCV14r6g4s1	N/A	10,867	0.11										
YCV14r6g5s1	N/A	10,461	0.10	3.24	0.22	4.1	0.01	146	34	26			
YCV14r7g5s1	N/A	10,461	0.13	3.52	0.2	4.3	0.01	162	35	26			
YCV14r7g4s1	N/A	10,050	0.09										
YCV14r7g2s1	N/A	11,134	0.07	3.46	0.18	4.24	0.02	160	30	23			
YCV14r7g1s1	N/A	10,919	0.08	4.00	0.28	4.59	0.01	200	70	42			
Pitchstone Plateau flow													
YCV12_r7g2s1	N/A	10,200	0.05	3.05	0.1	4.73	0.01	93	7	7			
YCV12_r7g3s1	N/A	10,690	0.06	3.41	0.21	5.71	0.01	83	11	10			
YCV12_r7g1s1	N/A	10,339	0.05	4.39	0.16	4.85	0.01	233	47	32			
YCV12_r6g1s1	N/A	9,751	0.09	2.17	0.14	3.43	0.01	80	14	12			
YCV12_r6g2s2	N/A	10,567	0.05										
YCV12_r6g6s1	N/A	11,010	0.05	6.03	0.3	6.17	0.01	383	–	117			
YCV12_r6g7s1	N/A	10,507	0.04	3.18	0.17	5.34	0.01	81	9	8			
YCV12_r6g9s1	N/A	10,808	0.05	3.70	0.23	5.8	0.02	95	13	12			
YCV12_r7g10s1	N/A	10,556	0.05	3.31	0.13	5.02	0.01	99	9	8			
YCV12_r4g4s1	N/A	10,534	0.04	3.78	0.22	5.48	0.01	110	16	14			
YCV12_r4g5s1	N/A	10,602	0.05	1.64	0.1	2.14	0.07	106	37	25			
YCV12_r3g8s1	N/A	10,331	0.06	3.83	0.15	5.05	0.01	136	15	13			
YCV12_r5g9s1	N/A	10,762	0.04										
YCV12_r5g9s2	N/A	11,354	0.06	3.66	0.17	5.16	0.01	116	13	12			
YCV12_r5g9s3	N/A	10,842	0.05	5.02	0.24	5.22	0.02	325	–	83			
Scaup Lake flow													
YCV08_g2s1@s1	N/A	12,041	0.13										
YCV08_g1s1@s1	N/A	12,041	0.04										
YCV08_g0s1@s1	N/A	11,448	0.15										
YCV08_g4s1@s1	N/A	10,854	0.22										
YCV08_g5s1@s1b	N/A	11,617	0.13										
YCV08_g8s1@s2	N/A	11,956	0.22										
YCV08_g12s1@s1	N/A	11,617	0.14										
YCV08_g14s1@s2	N/A	13,398	0.11										
West Yellowstone flow													
YCV09_r11g1s1	N/A	11,070	0.05	4.59	0.18	5.63	0.01	159	20	17			
YCV09_r9g8s1	N/A	11,787	0.10										
YCV09_r8g8s1	N/A	10,890	0.05	3.34	0.13	4.5	0.01	118	12	11			
YCV09_r8g6s1	N/A	11,052	0.07	4.11	0.18	5.26	0.01	139	17	15			
YCV09_r8g4s1	N/A	11,033	0.05	5.35	0.25	6.4	0.01	173	28	22			
YCV09BG_r3g10s2c	N/A	12,096	0.06	4.08	0.12	4.31	0.01	256	53	36			
YCV09BG_r3g10s3r	N/A	11,006	0.05	4.58	0.28	5.7	0.01	153	30	23			
YCV09BG_r3g8s1	N/A	11,110	0.06	3.9	0.18	4.14	0.01	247	81	46			

Table 1 continued

Analysis name	Zircon pop.	Hf (ppm)	Eu/ Eu*	(^{230}Th)/ (^{232}Th)	±1σ	(^{238}U)/ (^{232}Th)	± 1σ	Age (ka)	+ 1σ	− 1σ	ε_{Hf}	± 2σ	δ^{18}O (‰)
YCV09BG_r3g7s1r	N/A	11,007	0.08	3.74	0.25	4.24	0.01	192	65	40			
YCV09BG_r3g7s3c	N/A	11,032	0.09	3.2	0.15	3.78	0.01	163	30	23			
YCV09BG_r3g6s2r	N/A	10,787	0.06	4.07	0.15	4.57	0.01	201	32	25			
YCV09BG_r3g5s1c	N/A	11,198	0.06	3.94	0.25	4.61	0.01	175	46	32			
YCV09BG_r3g4s1c	N/A	11,778	0.10	4.46	0.21	4.5	0.01	351	–	99			
YCV09BG_r3g4s2r	N/A	11,293	0.07	3.56	0.19	4.72	0.01	125	18	16			
YCV09BG_r3g3s1r	N/A	9,992	0.10	5.10	0.32	5.78	0.01	202	60	38			
YCV09BG_r3g10s1@s2	N/A	11,872	0.10	4.08	0.12	4.31	0.01	256	53	36			
YCV09BG_r3g10s1@s3	N/A	11,363	0.09	4.58	0.28	5.7	0.01	153	30	23			
YCV09BG_r3g8s1@s1	N/A	11,956	0.07	3.9	0.18	4.14	0.01	247	81	46			
YCV09BG_r3g7s1@s3	N/A	12,211	0.09	3.2	0.15	3.78	0.01	163	30	23			
YCV09BG_r3g6s1@s1a	N/A	11,448	0.07	4.07	0.15	4.57	0.01	201	32	25			
YCV09BG_r3g5s1@s1c	N/A	11,702	0.06	3.94	0.25	4.61	0.01	175	46	32			

^{238}U–^{230}Th age data, selected trace-element data, oxygen isotopic data, and Hf isotopic data for Yellowstone zircons. Each row consists of the age, oxygen isotopic, Hf isotopic, and selected trace-element data for an individual zone within a zircon. For the ^{238}U–^{230}Th age columns, a dash mark is used to indicate secular equilibrium. The trace-element population classification of each zircon is included in the table ("Zircon Pop." column). Trace-element populations are reported only for HVF and SPF zircons, while "N/A" is reported for all other samples. *MR-like* main reservoir-like, *EC-like* extracaldera-like. For HVF and SPF zircons with no trace-element data, a "?" is included in the "zircon pop." column to indicate that the trace-element population is not known. U-series age data for all zircons from the Gibbon River flow, Dry Creek flow, West Yellowstone flow, and Pitchstone Plateau flow are from Vazquez and Reid (2002). U-series age data for SPF zircons with analysis names beginning in "SP(A)" are from Vazquez and Reid (2002). All other age data are from this study. Uncertainties in trace-element concentrations and U-series ages are discussed in Online Resource A1. Hf isotopic compositions of zircons are reported in terms of ε_{Hf}, calculated relative to $^{176}Hf/^{177}Hf_{CHUR(0)} = 0.282772$ (Vervoort and Blichert-Toft 1999). A combination of the Temora, 91500, and GJ1 zircon standards was analyzed after every 5–10 unknowns to assess the reproducibility of the Hf isotopic measurements. Uncertainties reported for the zircon Hf isotopic analyses are based on the 2σ reproducibility of the zircon standards run during the same day (see Online Resource A1 for more details). Uncertainties for oxygen isotopic compositions are not reported in this table, but are ±0.47 ‰ (2σ) based on the reproducibility of zircon standard 91500 run during the same day as the unknown analyses. Online Resource C2 contains the full zircon data set including all of the trace-element data, spot locations, and the instrumentation used for each analysis

field, GRF field, and in between the two (Fig. 6b). A small number of SPF zircon analyses plot within the Scaup Lake flow field.

Zircon O isotopic data

Oxygen isotopic data for zircons from the SPF and GRF are reported in Table 1, Fig. 7, and Online Resource C2. Figure 7 shows all oxygen isotopic data for GRF and SPF zircons. δ^{18}O values (‰ relative to standard mean ocean water) for GRF zircons dominantly range from 3.53 ‰ to 2.06 ‰, with one zircon analysis having a higher δ^{18}O (5.12 ‰). Most GRF zircons have δ^{18}O of ~3 ‰, but a few grains have δ^{18}O of ~2 ‰. When zoning is present, the cores of the GRF zircons have higher δ^{18}O than the corresponding rims (Fig. 7). SPF zircons have δ^{18}O values ranging from 4.17 to 1.67 ‰. Similar to zircons in the GRF, most SPF zircons have δ^{18}O of ~3 ‰, but a few grains have δ^{18}O extending to ~2 ‰. One SPF zircon has slightly higher δ^{18}O than all other SPF zircons (~4 ‰), although not outside of analytical uncertainty. When oxygen isotopic zoning is present, the cores of the SPF zircons have higher δ^{18}O than the corresponding rims, similar to GRF zircons (Fig. 7).

Glass and zircon Hf isotopic data

The $^{176}Hf/^{177}Hf$ ratios of rhyolite glass from the HVF, SPF, West Yellowstone flow, Pitchstone Plateau flow, and Dry Creek flow, as well as $^{176}Hf/^{177}Hf$ for the GRF whole rock are reported in Table 2. With the exception of the SPF, the CPM rhyolite glasses have Hf isotopic compositions that overlap within two standard deviations, with a weighted mean ε_{Hf} value of -6.1 ± 0.2 (2σ; MSWD = 1.9). The SPF has a lower ε_{Hf} of -6.6 ± 0.2 (2σ). The GRF has a whole-rock ε_{Hf} value of -6.5 ± 0.4 (2σ).

The $^{176}Hf/^{177}Hf$ ratios of zircons from the HVF, SPF, and GRF measured by LA-MC-ICPMS are presented in Table 1, Fig. 8, and Online Resource C2. All uncertainties on Hf isotopic compositions reported in the text and figures are 2 standard deviations. Figure 8 shows all $^{176}Hf/^{177}Hf$ data for the SPF, HVF, and GRF zircons and illustrates the

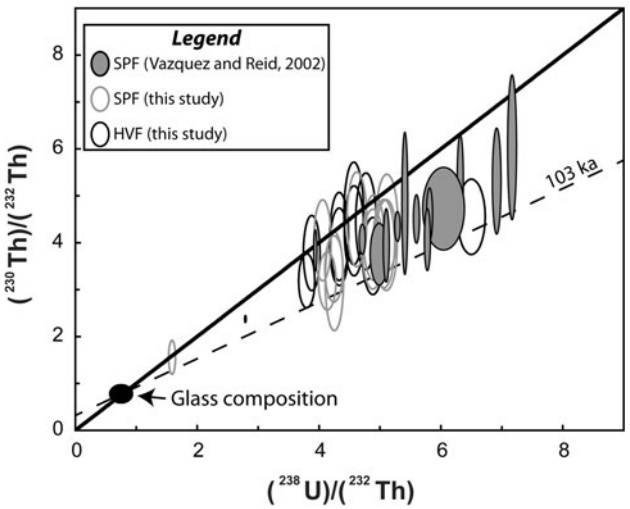

Fig. 5 ^{238}U–^{230}Th isochron diagram for zircons from the Solfatara Plateau flow and Hayden Valley flow rhyolites. *Each ellipse* represents a SHRIMP-RG analysis of a spot within a zircon grain. *Error ellipses* are 2σ. The *black filled ellipse* represents the glass (i.e., melt) composition used when calculating zircon model ages (see "Zircon trace-element concentrations and ^{238}U–^{230}Th ages" for explanation). The *solid black line* represents the equiline. The *dashed black line* is a reference isochron approximating the $^{40}Ar/^{39}Ar$ eruption age for the Hayden Valley flow and Solfatara Plateau flow rhyolites (Christiansen et al. 2007)

range of measured Hf isotopic compositions and general Hf isotopic zoning patterns within each sample. HVF zircons have ε_{Hf} ranging from −7.3 to 1.2, with an average of −4.2 ± 4.2 (2 SD). The HVF zircons often have cores with ε_{Hf} higher than the CPM glasses, but typically have rims that are within error of (or closer to) the composition of the host CPM glass. GRF zircons have a restricted range of Hf isotopic composition compared to SPF and HVF zircons, ranging from ε_{Hf} of −9.2 to −5.5, with a mean of −6.6 ± 1.8 (2 SD). All GRF rims (and most GRF cores) are within error of the GRF whole-rock value. Some GRF zircons have cores with ε_{Hf} values lower than the CPM glasses and GRF whole rock, but the GRF lacks zircons with ε_{Hf} higher than the CPM glasses. SPF zircons have ε_{Hf} ranging from −8.4 to 0.4, with a mean of −5.2 ± 3.9 (2 SD). The SPF zircons often have cores with ε_{Hf} higher than the CPM glasses (similar to HVF zircons), and one SPF zircon displays ε_{Hf} lower than the CPM glasses (similar to some GRF zircons). When zoned, the rims of SPF zircons have ε_{Hf} values more similar to the host glass than the corresponding core (Fig. 8).

Discussion

The trace-element data presented here document the presence of multiple zircon populations in the SPF and HVF rhyolites. However, interpretation of trace-element data is limited by uncertainty in the parameters controlling trace-element partitioning in zircon such as temperature, oxygen fugacity, melt chemistry, and kinetic effects during crystallization (see Burnham and Berry 2012; Reid et al. 2011; Schmitt 2011 and references therein; Trail et al. 2012). The addition of age and Hf isotopic data to the trace-element data allows us to infer the origin of Yellowstone zircon populations. An analogous approach was previously used by combining age and oxygen isotopic data (e.g., Bindeman et al. 2008; Valley 2003 and references therein; Watts et al. 2012). However, the new Hf isotopic data provide added insights into the origins of rhyolitic magmas at Yellowstone, particularly because the Hf isotopic

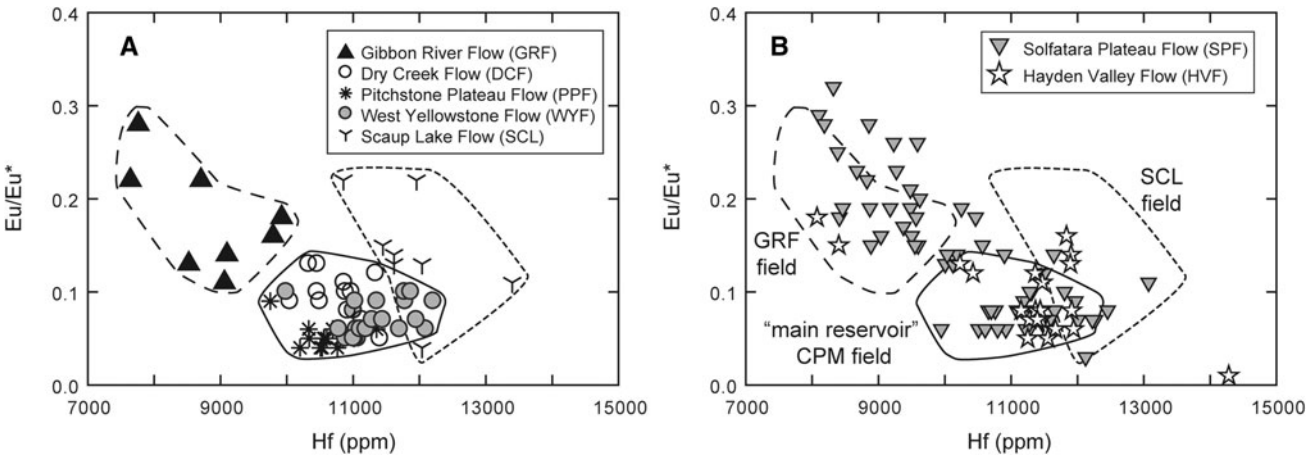

Fig. 6 Trace-element data for Yellowstone zircons. **a** Hf versus Eu/Eu* (Eu anomaly) for GRF, Dry Creek Flow, Pitchstone Plateau Flow, West Yellowstone Flow, and Scaup Lake flow zircons. The *solid line* encompasses all data from "main reservoir" CPM zircons. The *long dashed line* encompasses all zircon data from the extracaldera GRF. The *short dashed line* encompasses all zircon data from the Upper Basin Member (ca. 257 ka) Scaup Lake flow. **b** Hf versus Eu/Eu* for all HVF and SPF zircons. Reference fields for GRF zircons, "main reservoir" CPM zircons, and Scaup Lake flow zircons are included for comparison

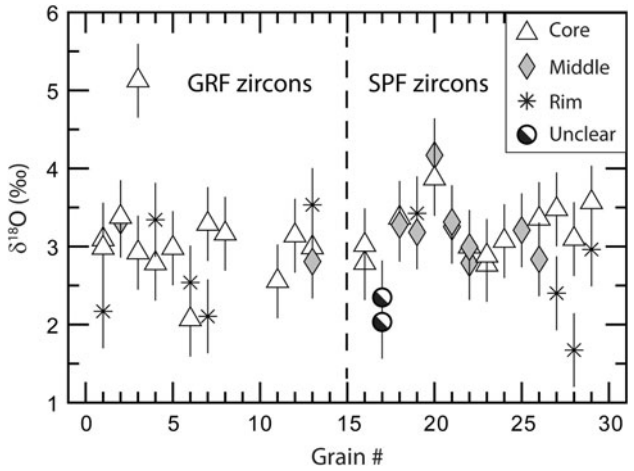

Fig. 7 $\delta^{18}O$ versus grain number for SPF and GRF zircons. All analyses from each zircon grain are stacked vertically so that zoning within grains can be visualized. Grain numbers on the *x*-axis are arbitrary and do not necessarily correspond to grain numbers in the data tables. *Symbols* correspond to the location within the grain of the oxygen isotopic analyses. Data from the SPF and GRF are separated by a vertical dashed line. Oxygen isotopic compositions are reported as $\delta^{18}O$, calculated relative to VSMOW. Uncertainties reported for unknown zircons are based on the external uncertainty of the zircon standard run during the same day. Note that (1) SPF and GRF zircons have nearly identical ranges of zircon $\delta^{18}O$ values and (2) several grains from the SPF and GPF display intragrain oxygen isotopic zoning from higher $\delta^{18}O$ cores to lower $\delta^{18}O$ rims

composition of zircon is a robust reflection of its parental melts due to insignificant diffusion at magmatic temperatures over timescales of millions of years (Cherniak and Watson 2003) and a resistance to hydrothermal alteration. Thus, Hf isotopic data can provide a sensitive indicator and robust record of juvenile versus evolved magma compositions despite a protracted and/or complex magmatic history. Similarly, we link major-element and Ba concentrations of sanidine crystals with their Pb isotopic compositions to identify distinct sanidine populations and infer the Pb isotopic composition and relative Ba concentrations of the melts from which they crystallized.

Zircon populations in the Solfatara Plateau flow and Hayden Valley flow

Defining zircon populations

We define zircon populations in the SPF and HVF based on how their Hf concentrations and Eu/Eu* compare to (1) zircons from "main reservoir" CPM rhyolites erupted through time, as represented by the Dry Creek flow, West Yellowstone flow, and Pitchstone Plateau flow; (2) zircons from the extracaldera GRF rhyolite; and (3) zircons from the Scaup Lake flow as representative of the Upper Basin Member rhyolites (Fig. 9). We define zircon populations using Hf concentrations and the Eu anomaly because they are the known indices of chemical fractionation (i.e., have predictable behavior in an evolving magma system; see Claiborne et al. 2010b; Schmitt 2011; Trail et al. 2012) and result in a clear separation between the different reference fields (Fig. 6, Fig. 9). We use zircons from "main reservoir" CPM rhyolites, an Upper Basin Member rhyolite, and an extracaldera rhyolite as points of comparison because these rhyolites represent the diversity of magma compositions erupted at Yellowstone after caldera collapse.

"Main reservoir-like" zircons are defined as grains for which all trace-element analyses lie within the "main reservoir" CPM field. "Extracaldera-like" zircons are defined as grains for which all trace-element analyses lie in the GRF field or in a few cases slightly above it (because low Hf concentration and high Eu/Eu* are characteristic of the GRF zircons). "Mixed" zircons are defined as grains for which any of the trace-element analyses for that grain lies within the region between the CPM and GRF fields or has zones that lie in both the CPM and GRF fields. A fourth population of zircons, called "inherited" zircons due to their similarities to zircons in the older Scaup Lake flow, are defined as grains for which any of the trace-element analyses lies outside of the "main reservoir" CPM field but within the Scaup Lake flow field. These population classifications represent robust geochemical groups because each zircon population also has distinct characteristics in terms of elements such as Eu, HREE, Ti, Y, U, and Th and element ratios such as Y/U and Eu/Lu (Online Resource B2 and C2).

One zircon in the HVF (HV-G3) has a resorbed core with a high Hf concentration, low Eu/Eu*, low Ti, and high REE + Y compared to all other zircons and does not lie in any of the defined fields (Fig. 9). The evolved trace-element composition of this zircon's core is consistent with crystallization in a highly fractionated melt (e.g., Bindeman et al. 2008; Miller and Wooden 2004), before being incorporated into the HVF magma. The core of this zircon has a young age (118^{+23}_{-19} ka) and ε_{Hf} (−5.1) within error of the CPM glasses, suggesting it may have been derived from a largely crystalline portion of the main CPM reservoir. This zircon is not considered further in the discussion because it does not clearly relate to the zircon populations outlined above.

The origin of young zircon populations at Yellowstone

Each zircon trace-element population also has distinct age and Hf isotopic characteristics, implying distinct origins for the different zircon populations (Figs. 10, 11). Main reservoir-like zircons in the HVF and SPF display (1) a broad range of ε_{Hf} (0.2 to −7.4), (2) distinct trace-element characteristics compared to extracaldera-like and

Table 2 Hf isotopic compositions of the CPM rhyolite glasses and GRF whole rock

Sample	$^{176}Hf/^{177}Hf$	1 SE (analytical)	ε_{Hf}	$\pm\varepsilon_{Hf}$ (2 SE analytical)
CPM glasses and standards (Neptune Plus)				
Dry Creek flow	0.282599	0.000001	−6.12	0.08
Hayden Valley flow	0.282605	0.000001	−5.91	0.09
Pitchstone Plateau flow	0.282596	0.000002	−6.24	0.14
Solfatara Plateau flow	0.282585	0.000002	−6.61	0.12
West Yellowstone flow	0.282602	0.000002	−6.02	0.13
BCR-2	0.282869	0.000002	3.42	0.17
	0.282864	0.000003	3.26	0.24
	0.282868	0.000002	3.38	0.12
JMC-475	0.282147	0.000002	−22.11	0.11
	0.282141	0.000001	−22.32	0.10
Gibbon River flow whole rock and standards (Nu Plasma)				
Gibbon River flow (whole rock)	0.282587	0.000002	−6.54	0.15
AGV-2	0.282980	0.000002	7.34	0.15
BHVO-1	0.283109	0.000002	11.91	0.17
JMC-475	0.282150	0.000003	−22.01	0.20
	0.282145	0.000004	−22.17	0.32
	0.282156	0.000003	−21.77	0.21
	0.282151	0.000004	−21.96	0.31
	0.282160	0.000003	−21.64	0.21

Solution MC-ICPMS Hf isotopic data for Central Plateau Member rhyolites and the Gibbon River flow. Data from the two analytical sessions are separated in the table. ε_{Hf} is calculated relative to $^{176}Hf/^{177}Hf_{CHUR(0)} = 0.282772$ (Vervoort and Blichert-Toft 1999). $^{176}Hf/^{177}Hf$ ratios of all analyses reported here (except those of JMC-475) have been normalized to the conventionally accepted value of JMC-475 (0.282160; Vervoort and Blichert-Toft 1999). Uncertainties in the Hf isotopic compositions of the CPM rhyolites and GRF whole rock reported in the text are based on the reproducibility of the solution standards and rock standards run on the day of the analyses. Uncertainties for the session on the Neptune Plus are ±0.2 ε_{Hf}, and uncertainties for the session on the Nu Plasma are ±0.4 ε_{Hf}. See Online Resource A2 for details on the Hf isotopic analyses

"inherited" zircons, and (3) ages that are typically ≤250 ka (with the exception of 5 crystals within error of secular equilibrium; Figs. 10, 11; Table 1, and Online Resource C2). The cores of main reservoir-like zircons dominantly have higher and more variable ε_{Hf}, Eu, Y, HREE, U, and Th than the rims, and most rims have lower and more restricted trace-element concentrations and ε_{Hf} within error of the CPM glasses (Figs. 10a, 12a; Table 1, Online Resources B3 and C2). The variable trace-element concentrations and ε_{Hf} of the main reservoir-like zircon cores suggest that the zircons crystallized from multiple magmas with a range of ε_{Hf} (~0.2 to −7.4) and variations in either trace-element compositions or physical parameters. Main reservoir-like zircon cores with high ε_{Hf} (>−4.0) have crystallization ages ranging from within error of their respective $^{40}Ar/^{39}Ar$ eruption age to >250 ka (Fig. 11a, b), suggesting that their relatively high $^{176}Hf/^{177}Hf$ parental magma(s) is either (1) a long-lived (>100 ka) magma reservoir(s) or (2) isotopically similar batches of silicic melt that were periodically added to the reservoir over at least the time interval indicated by the zircon crystallization ages (i.e., >100 ka before eruption). In contrast to their cores, most main reservoir-like zircon rims have similar ε_{Hf} to the host CPM glasses and more restricted trace-element compositions, suggesting that the most recent zircon growth was from a more homogeneous liquid similar to the host CPM glasses (Fig. 10a).

"Inherited" zircons in the SPF and HVF have Eu/Eu* and Hf concentrations similar to main reservoir-like zircons (Fig. 9) but have a range of Eu and ε_{Hf} more similar to extracaldera-like zircons (Fig. 10). "Inherited" zircons have cores with higher Eu (>0.5 ppm) than main reservoir-like zircons and ε_{Hf} (−4.1 to −5.7) slightly higher than the host glass, whereas the rims are similar to most main reservoir-like zircon rims with low Eu (<0.5 ppm) and ε_{Hf} (−6.0 to −7.3). The distinct and more variable trace-element composition of "inherited" zircons compared to main reservoir-like zircons suggests that the two populations have distinct sources. Additionally, the cores of "inherited" zircons yield ages within error of secular equilibrium (i.e., >250 ka; Fig. 11 and Online Resource C2), suggesting they are derived from an older source.

Although main reservoir-like and "inherited" zircons have distinct trace-element compositions in their cores, the similarity in trace-element and Hf isotopic composition of "inherited" zircon rims with most main reservoir-like

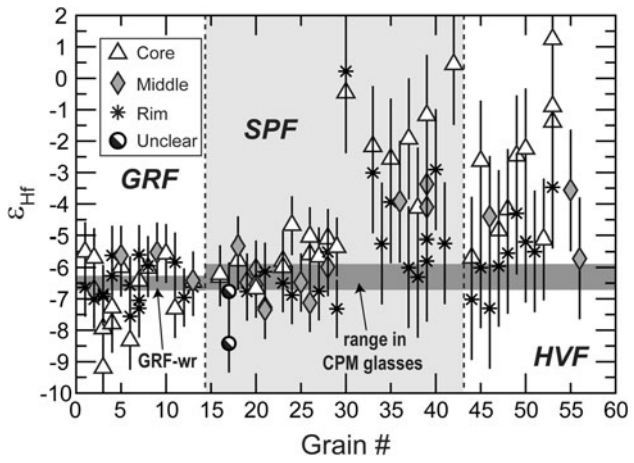

Fig. 8 ε_{Hf} versus grain number for SPF, HVF, and GRF zircons. All analyses from each zircon grain are stacked vertically so zoning within grains can be visualized. Grain numbers on the *x*-axis are arbitrary and do not correspond to grain numbers in the data tables. *Symbols* correspond to the location within the grain of the Hf isotopic analyses. Data from the SPF, HVF, and GRF are separated by vertical dashed lines, and the SPF zircons are shown with a gray background. In the HVF and SPF regions, the dark gray horizontal bar represents the range of Hf isotopic compositions of all CPM glasses presented in this study (including the SPF). In the GRF region, the dark gray bar represents the GRF whole-rock Hf isotopic composition with analytical uncertainty. Hf isotopic compositions are reported in terms of ε_{Hf}, calculated relative to $CHUR_{(0)} = 0.282772$ (Vervoort and Blichert-Toft 1999). Uncertainties reported for unknown zircons are based on the reproducibility (2 SD) of the zircon standards run during the same day (see Online Resource A1 for more details). Note that the HVF zircons often have cores with ε_{Hf} higher than the CPM glasses, but typically have rims that are within error of the composition of the host CPM glass. GRF zircons have a more restricted range of ε_{Hf} (compared to HVF zircons) that extends to lower values than the CPM glasses, but lacks zircons with ε_{Hf} higher than the CPM glasses. Lastly, note that the SPF contains several zircons that are similar to HVF zircons and some that are similar to GRF zircons. Intragrain Hf isotopic zoning outside of 2σ uncertainty is observed in several zircons from the SPF, HVF, and GRF

zircon rims suggests that both zircon populations experienced their final growth in a common magma reservoir, similar in composition to the CPM glasses (Fig. 10a, b). The interpretation that the main reservoir-like and "inherited" zircons were present within the main CPM reservoir is supported by the lack of main reservoir-like and "inherited" zircons in the extracaldera GRF, suggesting that these components are characteristic of the "main reservoir" rhyolites.

Extracaldera-like zircons (only found in the SPF) have age, trace-element, and Hf isotopic characteristics distinct from all other zircon populations in the SPF and HVF, but identical to zircons from the extracaldera GRF (Figs. 9, 10c, 11). The distinct trace-element composition of extracaldera-like zircons compared to main reservoir-like zircons suggests that the extracaldera-like zircons crystallized from magma distinct in trace-element composition and/or under different physical conditions than the main reservoir rhyolites. Extracaldera-like zircons lack high ε_{Hf} cores (>-5 ε_{Hf}), have a range of ε_{Hf} that is identical to zircons in the GRF, and for all but two analyses are within error of the GRF whole-rock Hf isotopic composition, which is consistent with the extracaldera-like zircons having the same origin as the GRF zircons (Fig. 10c). The presence of one zircon crystal with lower ε_{Hf} relative to the CPM glasses and GRF whole rock suggests that some extracaldera-like zircons may have crystallized from melts that are isotopically more "crustal" relative to the CPM glasses and GRF whole rock. The young age of the extracaldera-like zircons (ca. 117 ka to ca. 155 ka) rules out inheritance from older rhyolites (e.g., Upper Basin Member rhyolites, Huckleberry Ridge Tuff). KS tests using ^{238}U–^{230}Th age data demonstrate that extracaldera-like zircons in the SPF have an age spectrum indistinguishable from zircons in the extracaldera GRF; however, the null hypothesis (of derivation from the same population) is rejected 79–95 % of the time when extracaldera-like and GRF zircons are compared to (1) main reservoir-like zircons in the SPF/HVF, (2) zircons from older "main reservoir" CPM rhyolites (i.e., West Yellowstone flow and Dry Creek flow), and (3) "inherited" zircons in the SPF/HVF, consistent with a distinct age distribution relative to the other zircon populations (Fig. 11). Considered together, these age, trace-element, and Hf isotopic data indicate that GRF zircons and extracaldera-like zircons from the SPF share a common source that is distinct in age and composition from the main CPM reservoir.

Mixed zircons display trace-element and Hf isotopic characteristics of both main reservoir-like and extracaldera-like zircons and have ages that define a broad, unimodal probability density function (PDF) with a model age peak that lies between those for main reservoir-like and extracaldera-like zircons. Trace-element data demonstrate that mixed zircons have cores with main reservoir-like, extracaldera-like, and intermediate compositions, but rims on most mixed grains are intermediate in composition relative to the CPM and GRF fields, suggesting that the CPM reservoir mixed with extracaldera magma and zircon rims of a hybrid composition grew on some main reservoir-like and extracaldera-like zircon cores (Fig. 12).

It is noteworthy that all of the zircon data presented in this study are from analyses of polished cross sections of the zircons, which may bias the results toward the early part of zircon growth, and analyses of unpolished crystal faces or continuous depth profiling may better capture the final stages of zircon growth (e.g., Reid et al. 2011; Storm et al. 2012). Accordingly, it is possible that some of our zircon "rim" analyses that do not have ε_{Hf} within error of the CPM rhyolite glasses reflect the spatial resolution of the laser ablation analysis pit ($\sim$50 μm diameter by $\sim$25 μm

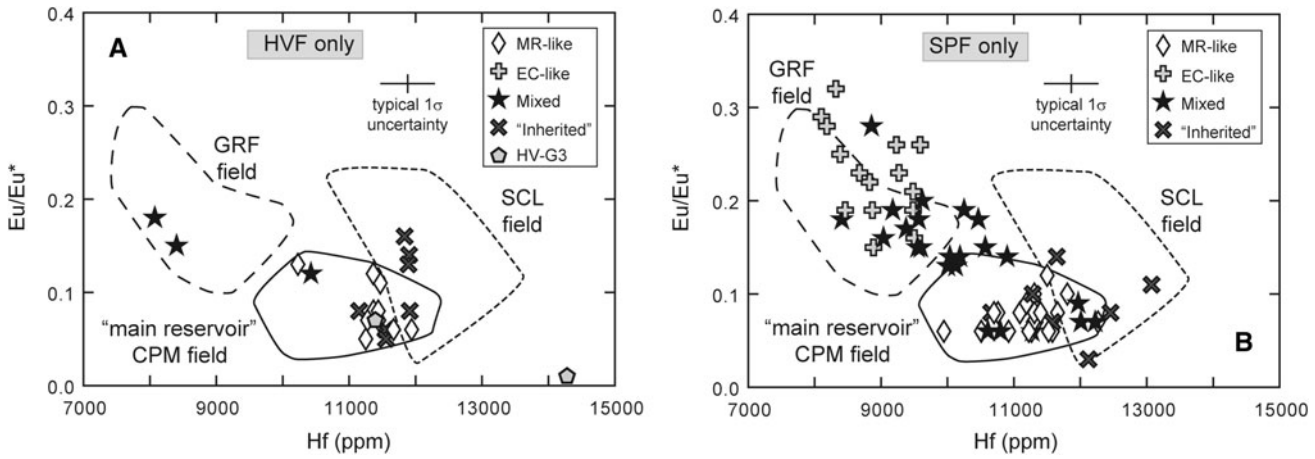

Fig. 9 Defining zircon populations in the HVF and SPF based on Hf (ppm) versus Eu/Eu*. *Symbols* correspond to the different zircon populations as defined in the text ("Defining zircon populations"). *MR-like* main reservoir-like, *EC-like* extracaldera-like. Reference fields for GRF zircons, "main reservoir" CPM zircons, and Scaup Lake flow zircons are those defined in Fig. 3. One zircon from the HVF (HV-G3, plotted with a *unique symbol*) does not fit in any of the defined zircon populations and is not considered further. Conservative 1σ uncertainties on Hf (ppm) and Eu/Eu* are <4 and <10 %, respectively (see Online Resource A1 for more details). See text for discussion

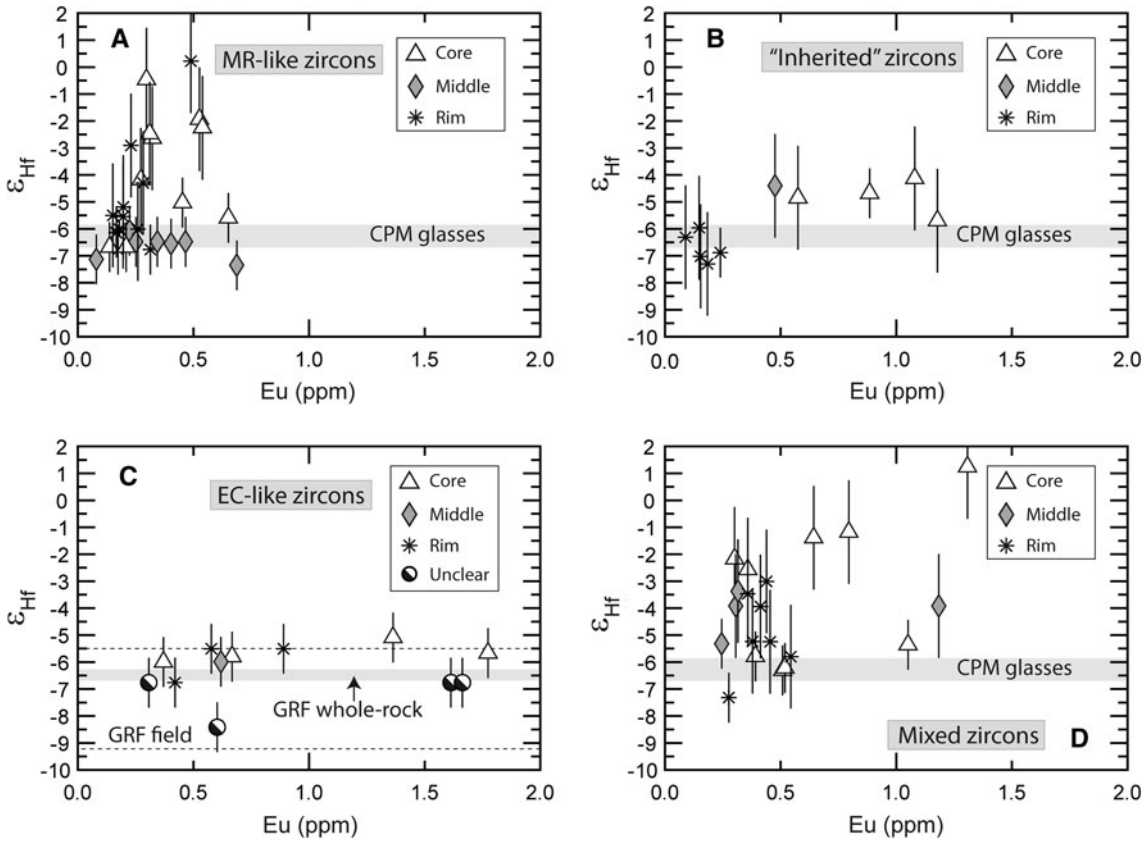

Fig. 10 Eu (ppm) versus ε_{Hf} for HVF and SPF zircons. **a** Main reservoir-like zircons from the HVF and SPF. **b** "Inherited" zircons from the HVF and SPF. **c** Extracaldera-like zircons from the SPF. **d** Mixed zircons from the SPF (one grain from the HVF). *Symbols* correspond to the location of the analysis spots. *Error bars* for the Hf isotopic analyses show 2σ uncertainties. Conservative 2σ uncertainties on Eu concentrations are <20 % (see Supplementary Material A1 for more details). The *gray bars* in **a**, **b**, and **d** represent the range of Hf isotopic compositions for all CPM glasses measured in this study (including the SPF glass). In **c** the *short dashed region* encompasses all data for zircons from the extracaldera GRF, and the *gray bar* represents the GRF whole-rock Hf isotopic composition

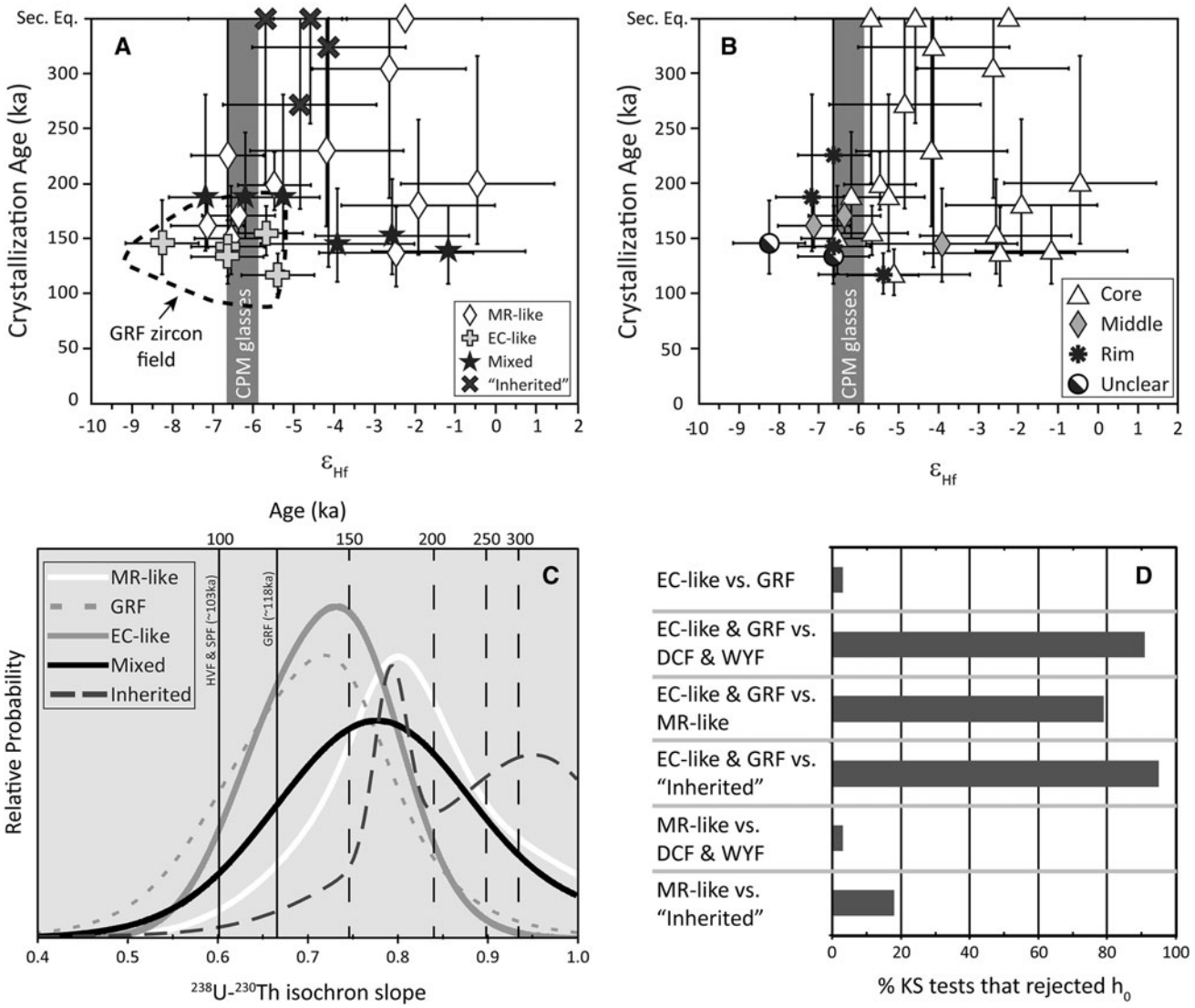

Fig. 11 Zircon age and Hf isotopic data. All data points displayed here represent LA-MC-ICPMS Hf isotopic analysis and SHRIMP-RG ^{238}U–^{230}Th dating of the same zone within a zircon. **a** ε_{Hf} versus crystallization age (ka) for SPF and HVF zircons. *Symbols* represent the trace-element populations of the zircons (see "Defining zircon populations" for explanation). The *long dashed field* encompasses all zircon data from the Gibbon River flow (GRF). **b** ε_{Hf} versus crystallization age (ka) for SPF and HVF zircons. *Symbols* represent the location of the Hf isotopic and age analyses within the zircon grain. The relative paucity of zircon rim analyses compared to core analyses in panel B reflects the difficulty in measuring ^{238}U–^{230}Th ages on the zircon rims due to low U concentrations and young ages (Online Resource A1). **c** Probability density functions (PDF) for zircon age data from the SPF, HVF, and GRF (GRF data from Vazquez and Reid 2002). Each PDF corresponds to a different zircon population. *Vertical solid lines* represent the eruption ages of the HVF, SPF, and GRF (from Christiansen et al. 2007). *Vertical dashed lines* are reference lines linking the slope of the isochron to an absolute age. **d** Results of the KS tests comparing zircon age data from different populations/samples. The *Y*-axis shows the different zircon populations being compared in the KS test. The *bars* represent the percent of the time that the KS test rejected the null hypothesis (h_0) during the Monte Carlo simulation (i.e., the percentage of trials inconsistent with the two populations being compared being derived from the same age distribution). For the *p* values used in the KS test to be robust, the following must be true: $(n_{\text{Sample 1}} \times n_{\text{sample 2}})/(n_{\text{Sample 1}} + n_{\text{sample 2}}) \geq 4$, where $n_{\text{Sample 1}}$ is the number of analyses in sample 1 and $n_{\text{Sample 2}}$ is the number of analyses in sample 2. All of the KS tests in **d** meet this requirement except for when comparing extracaldera-like and GRF zircons. However, the indistinguishable trace-element and Hf isotopic compositions of extracaldera-like and GRF zircons suggest that these zircons are from the same population (see "The origin of young zircon populations at Yellowstone" for explanation), supporting the KS test results. We combine the extracaldera-like and GRF zircon data sets for the rest of the KS tests to ensure that there were enough age analyses for the KS tests to be robust. Abbreviations used in the figure are defined as follows: *MR-like* main reservoir-like, *EC-like* extracaldera-like, *DCF* Dry Creek flow, *WYF* West Yellowstone flow, *GRF* Gibbon River flow

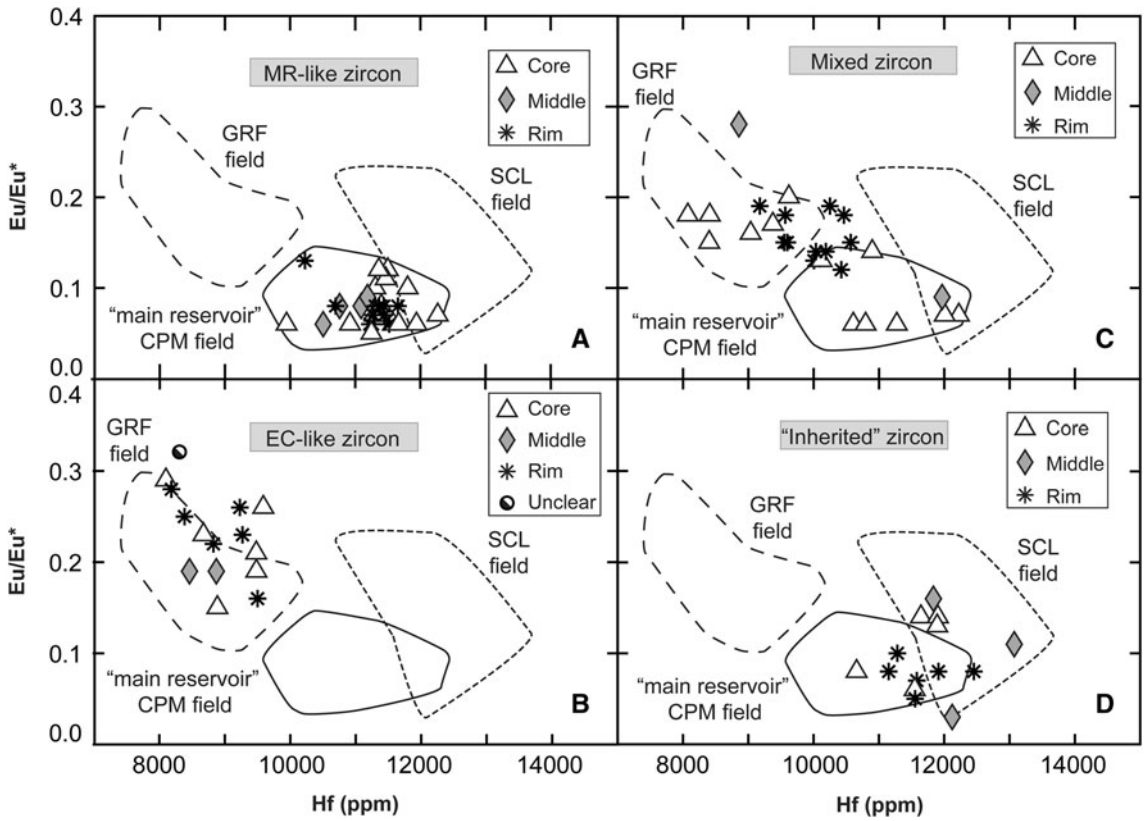

Fig. 12 Hf (ppm) versus Eu/Eu* for the different zircon populations in the HVF and SPF, illustrating core to rim variations in trace-element composition. *Each panel* corresponds to zircons from a specific zircon population. *Symbols* correspond to the location of the trace-element analysis within the zircon grain. Reference fields are those defined in Fig. 3. See "Zircon populations in the Solfatara Plateau flow and Hayden Valley flow" for discussion

deep pit) and its potential for integrating multiple growth zones.

Sanidine populations in the Solfatara Plateau flow and Hayden Valley flow

EMP and LA-MC-ICPMS analyses of sanidines demonstrate that the SPF and HVF have distinct sanidine populations, with different major-element compositions, Ba concentrations, and Pb isotopic compositions (Figs. 3, 4). SPF and HVF sanidines also display different patterns of core to rim zonation in Ba concentration and Pb isotopic composition (Fig. 13). HVF sanidines are either unzoned in Ba or display normal zoning from high-Ba cores to low-Ba rims (concentration differences on the order of a few hundred to 1,000 ppm), consistent with closed-system crystallization of the sanidine-rich phenocryst assemblage in the HVF magma (Fig. 13). Furthermore, HVF sanidines have homogeneous Pb isotopic compositions that are identical to their host HVF glass, indicating that HVF sanidines are autocrysts that wholly crystallized from their host melt (Figs. 4, 13b, 14).

The SPF sanidines define three populations based on Ba zonation—one with no Ba zoning, one with extreme zoning from low-Ba cores (~2,000 to 4,000 ppm) to high-Ba rims (~6,000 to 8,000 ppm), and several sanidines with relatively high (~10,000 ppm) Ba cores that are mantled by lower Ba (~7,000 ppm) rims (Fig. 13a). SPF sanidines lacking Ba zonation, or with cores higher in Ba concentration than the corresponding rims, have Pb isotopic compositions that are within error of their host SPF glass, which is consistent with growth from the SPF glass or an isotopically identical melt (Fig. 13). On the other hand, SPF sanidines that are zoned from low-Ba cores to high-Ba rims also commonly display zoning in Pb isotopic composition, such that the low-Ba cores correspond to lower $^{208}Pb/^{206}Pb$ and $^{207}Pb/^{206}Pb$ (Figs. 13, 14). This requires that many of the low-Ba SPF sanidine interior zones did not grow from the liquid represented by the host SPF glass. The broad correlation between Ba concentration and Pb isotopic composition displayed by SPF sanidines suggests that changes in Ba concentration in the SPF sanidines largely reflect changes in the composition of the melts from which the sanidines crystallized (Fig. 14). Some of the

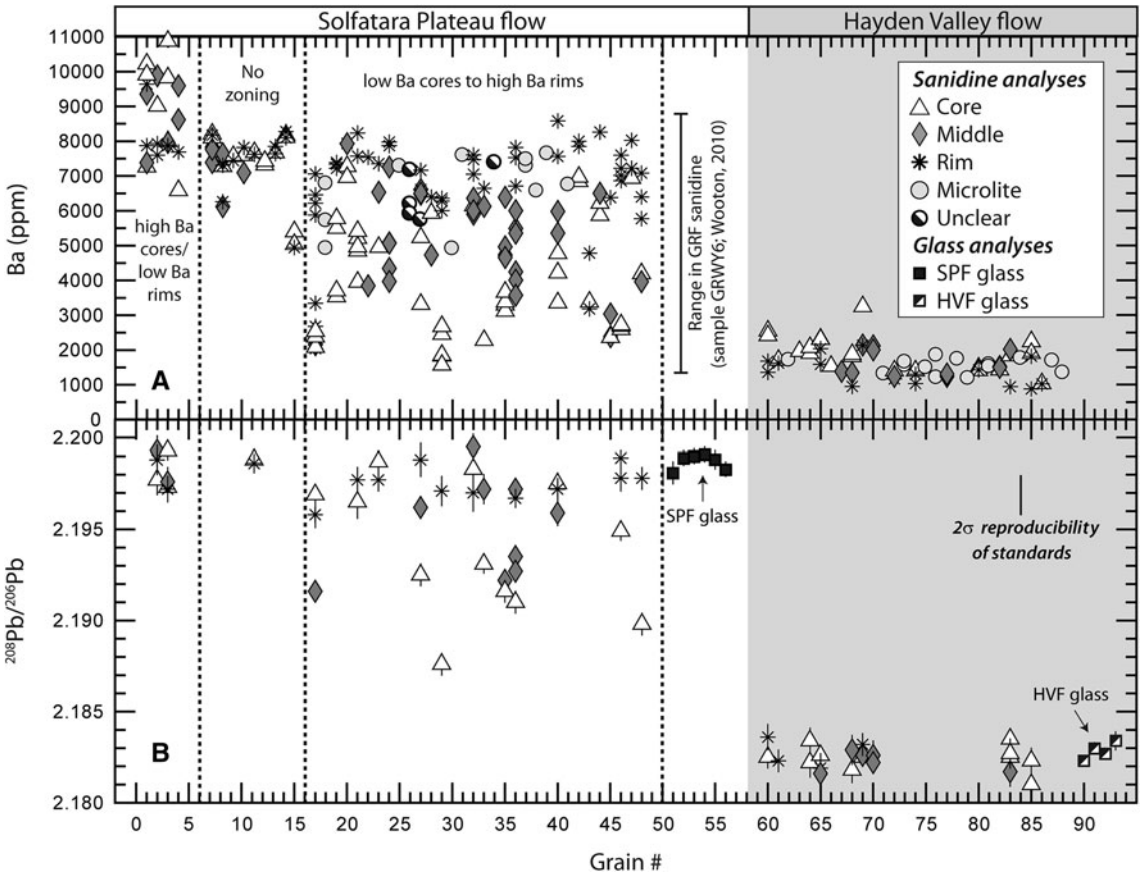

Fig. 13 Visualizing zoning patterns in Ba concentration and Pb isotopic composition within SPF and HVF sanidine crystals. **a** Ba (ppm) versus grain number. *Each data point* is an electron microprobe analysis of a 10-µm-diameter zone within a sanidine grain. **b** $^{208}Pb/^{206}Pb$ versus grain number. *Each data point* is a LA-MC-ICPMS analysis of a 100-µm-diameter zone within a sanidine grain. LA-MC-ICPMS spots were located on the top of the spots previously analyzed by EMP, so the data in **a** and **b** may be directly compared. In both *panels*, all analyses from each sanidine grain are stacked vertically so intragrain zoning in Ba concentration and $^{208}Pb/^{206}Pb$ can be visualized. Grain numbers on the *x*-axis are arbitrary (used to group different populations in the SPF) and do not necessarily correspond to grain numbers in the data tables. *Symbols* correspond to the location of the EMP and LA-MC-ICPMS analyses within the sanidine crystal. Sanidines from the SPF and HVF are located in the areas shaded *white* and *gray*, respectively. *Vertical dashed lines* separate different crystal populations for the SPF (based on Ba zoning patterns). 2σ uncertainties on individual Ba concentrations range from 200 to 400 ppm (approximately the size of the symbols in **a**). Uncertainties in $^{208}Pb/^{206}Pb$ shown with the data points are the 1 SE analytical uncertainty. The reproducibility (2 standard deviations) of the external check standard (NIST 612) is included in the upper right-hand corner of **b** and represents a more conservative estimate of the uncertainty for an individual analysis. See "Sanidine populations in the Solfatara Plateau flow and Hayden Valley flow" for discussion

scatter in this correlation is likely due to the much larger volume of material sampled during the LA-MC-ICPMS analyses compared to the EMP analyses. Despite the variability of Ba concentrations and Pb isotopic compositions for SPF sanidine cores, all SPF sanidines have rims with a relatively restricted range of Ba concentrations compared to the cores [averaging 7,031 ± 2,489 ppm (2 SD)], and Pb isotopic compositions within error of their host SPF glass (Fig. 13). Thus, the data for SPF sanidine rims indicate that all SPF sanidines experienced final growth in a common magma represented by the SPF glass.

Taken together, the Ba concentrations and Pb isotopic compositions of SPF sanidines clearly indicate that many SPF sanidines grew from multiple, chemically and isotopically distinct rhyolites over their lifetime before final growth in the magma represented by the SPF glass. The zoning in Ba concentration and Pb isotopic composition displayed in many SPF sanidines is typically abrupt with sharp contacts between zones of different Ba concentrations and Pb isotopic compositions (sometimes displaying resorption textures). Some large SPF sanidines show evidence for at least three distinct zones that have unique Ba concentrations and Pb isotopic compositions, with sharp contacts between each zone (e.g., Fig. 15). These observations suggest that the changes in magma composition were periodic and abrupt, implying that new pulses of magma were injected into the region of the magmatic system where the SPF sanidines were growing

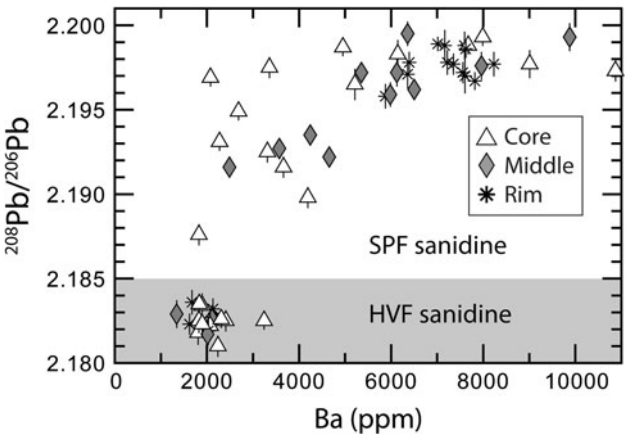

Fig. 14 $^{208}Pb/^{206}Pb$ versus Ba (ppm) for SPF and HVF sanidines. All HVF sanidines lie in the region with a gray background, and all SPF sanidines lie in the region with a white background. *Each data point* represents an EMP analysis for Ba concentration and LA-MC-ICPMS analysis for Pb isotopic composition of the same zone within a sanidine grain. *Symbols* correspond to the location of the analyses within the sanidine grain. Note that the HVF sanidines have homogeneous Ba concentrations and $^{208}Pb/^{206}Pb$ ratios, consistent with crystallization from the HVF glass. Also note that SPF sanidines have rims with homogeneous Pb isotopic compositions and restricted Ba concentrations, but SPF sanidine cores and middles display a wide range of Pb isotopic compositions and Ba concentrations. Many SPF sanidines have cores (and middles) with lower $^{208}Pb/^{206}Pb$ ratios and lower Ba concentrations that are more similar to HVF sanidines

and/or that some cores of SPF sanidines are antecrystic (i.e., derived from a genetically related but compositionally distinct magma). Despite the heterogeneity preserved in some SPF sanidine interiors, the homogeneous rim compositions of all SPF sanidines demonstrate that the SPF magma was homogenized prior to eruption. The presence of some SPF sanidines without Ba or Pb isotopic zonation suggests that these sanidines started to grow after the SPF magma was homogenized.

Mixing of Yellowstone's intra- and extracaldera rhyolite

Comparing crystal populations within the coeval SPF and HVF rhyolites leads to important insights about the origin of the compositionally anomalous SPF and its relationship to the main reservoir CPM rhyolites, as well as the petrologic signature of magma mixing in the Yellowstone magma reservoir. The HVF (1) has glass with a trace-element and isotopic composition similar to other main reservoir CPM rhyolites, (2) lacks extracaldera-like zircons, (3) is dominated by main reservoir-like and "inherited" zircons, and (4) contains a single sanidine population with low Ba concentrations and Pb isotopic compositions in equilibrium with the host HVF glass. All of these observations are consistent with derivation of the HVF from the main CPM reservoir (Fig. 16). In contrast, the SPF has roughly equal proportions of main reservoir-like, mixed, and extracaldera-like zircons with a minority of "inherited" zircons, suggesting that the SPF represents a mixture of main reservoir CPM magma (similar to the HVF) with extracaldera magma similar to the GRF. The presence of

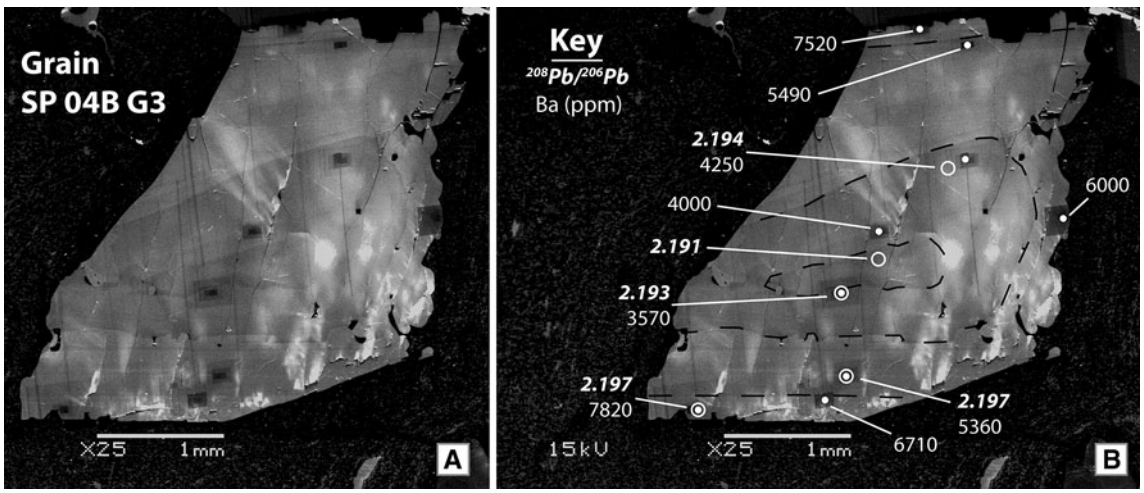

Fig. 15 Cathodoluminescence image of SPF sanidine grain (SP 04B G3) displaying multiple zones of distinct Pb isotopic composition and Ba concentrations. This image was taken after EMP analyses but before LA-MC-ICPMS analyses. The sanidine in this image is surrounded by the groundmass glass. **a** The unedited image and **b** the annotated image of the same grain shown in **a**. The *open white circles* in **b** represent the locations of the LA-MC-ICPMS Pb isotopic analyses. The *filled white circles* in **b** represent the locations of the EMP analyses for major-element and Ba concentrations. The *black dashed lines* in **b** mark the boundaries between the zones of different CL brightness within the sanidine crystal. *Bright areas*/streaks on the grain reflect charging due to the carbon coat being too thin in those areas. *Dark rectangular areas* on the sanidine grain are from EMP scans of the area prior to EMP analysis. Note the systematic zoning from a low-Ba and low $^{208}Pb/^{206}Pb$ core to high-Ba and high $^{208}Pb/^{206}Pb$ rim, and how zones of similar CL brightness have similar Pb isotopic compositions and Ba concentrations. Also note that the contacts between zones are sharp and sometimes show resorption textures. Uncertainties on Pb isotopic compositions are ±0.001 (2σ). Uncertainties in Ba concentrations are ±200 to 400 ppm (2σ)

multiple sanidine populations in the SPF is consistent with its multiple zircon populations and suggests that the SPF is a mixture of at least two distinct magmas. The SPF sanidine data require that one of the mixing end-members is characterized by high Ba concentrations, high $^{208}Pb/^{206}Pb$, and high $^{207}Pb/^{206}Pb$ relative to the other mixing component (Figs. 13, 14). The observation that many SPF sanidines with low-Ba cores also have lower $^{208}Pb/^{206}Pb$ and $^{207}Pb/^{206}Pb$ that is more similar to the HVF sanidine/glass is consistent with the low-Ba, low $^{208}Pb/^{206}Pb$, and low $^{207}Pb/^{206}Pb$ mixing end-member being main reservoir CPM magma (Fig. 14).

Considered together, the SPF and HVF sanidine and zircon data are consistent with the SPF representing a mixture of main reservoir magma similar to the HVF with extracaldera magma similar to the GRF. From a mass balance perspective, explaining the SPF as a mixture of extracaldera magma similar to the GRF with a main reservoir CPM rhyolite requires that the extracaldera magma has (1) a trace-element composition complementary to the HVF (i.e., such that the SPF has trace-element concentrations between the HVF and GRF) and (2) lower $\delta^{18}O$ and ε_{Hf} relative to the SPF glass. These requirements are seemingly at odds with trace-element and isotopic data for the GRF published in Hildreth et al. (1984) and Hildreth et al. (1991), but recent studies indicate that the GRF is compositionally zoned. Wooton (2010) documented that the GRF contains a wide range of whole-rock trace-element concentrations (e.g., Ba ranges from ~19 to ~880 ppm) and likely comprises multiple flow units that potentially represent distinct magma batches. One flow unit of the GRF represents a viable end-member that could produce the SPF if mixed with a "main reservoir" CMP rhyolite, as it (1) has an almost identical composition to the SPF glass in all trace elements except for having higher Ba (878 ppm), Sr, Eu, and Eu/Eu*, (2) contains zircons with an age distribution indistinguishable from that reported for the GRF zircons in Vazquez and Reid (2002) and EC-like zircons in this study, and (3) contains sanidines with a range of major-element composition and Ba concentration similar to sanidines in the SPF (Fig. 13; Wooton 2010). Hf isotopic data presented here support this mixing scenario because the GRF whole rock has an ε_{Hf} value within error of the SPF glass and lower than the "main reservoir" CPM glasses. Additionally, oxygen isotopic data from GRF zircons are consistent with this mixing scenario because the GRF zircons have low $\delta^{18}O$ values similar to SPF zircons analyzed in this study and to main reservoir CPM zircons reported in Watts et al. (2012), indicating that the GRF magma itself must have a low $\delta^{18}O$ value (Fig. 7). Thus, although the GRF is apparently ~15 ka older than the SPF and HVF (Christiansen et al. 2007) and therefore may not itself represent the extracaldera magma involved in generating the SPF, these data demonstrate that the GRF or extracaldera magma akin to the GRF (or perhaps residual magma from the GRF eruption) could produce the SPF if mixed with a "main reservoir" CPM rhyolite similar to the HVF.

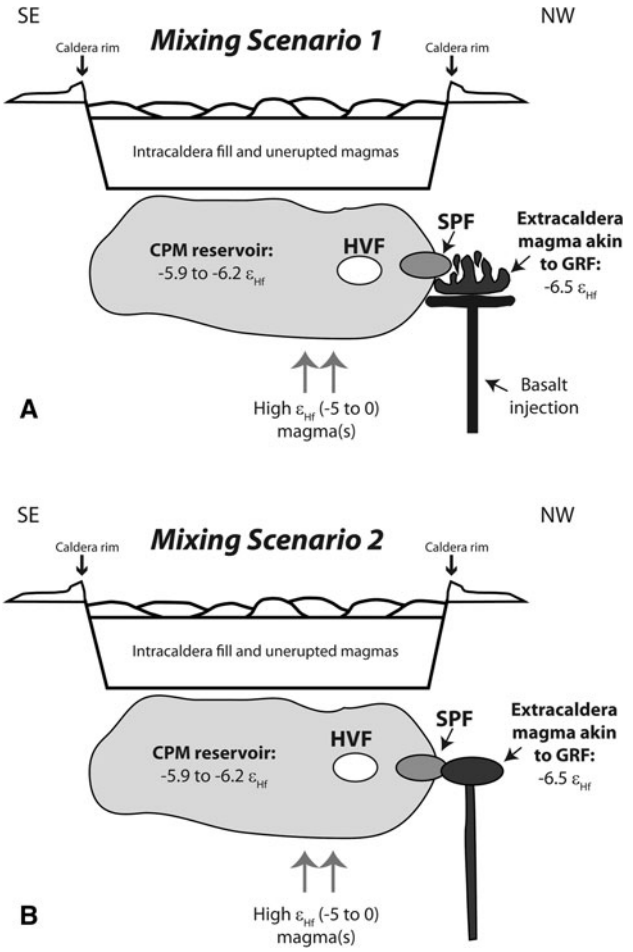

Fig. 16 Models for the formation of the SPF and HVF rhyolites. The models represent a schematic cross section across the caldera from SE to NW along the eastern vent lineament (see Fig. 1). The size and depth of the main CPM reservoir, HVF magma, SPF magma, and extracaldera magma are purely schematic. The only physical constraint is that mixing between the main CPM reservoir and extracaldera magma must have occurred at the margin of the main CPM reservoir. **a** Mixing Scenario 1. The SPF magma was generated when the margin of the CPM reservoir and the adjacent extracaldera source rock were melted due to basaltic underplating and subsequently mixed. **b** Mixing Scenario 2. The SPF magma was generated when dominantly liquid extracaldera magma ascended from depth and mixed with the margin of the CPM reservoir. See text for a detailed description of the mixing scenarios. In both mixing scenarios, the HVF is erupted from the main CPM reservoir and the SPF is erupted from a hybrid magma that is a mixture of extracaldera magma with the margin of the CPM reservoir. In both *panels* the *dark gray* magma represents extracaldera magma similar to the GRF, the *medium gray* oval represents the erupted SPF magma, the *light gray* region represents the main CPM reservoir, and the *white oval* represents the erupted HVF magma. The high ε_{Hf} magma represents the magma that provided the main reservoir-like zircons with high ε_{Hf} cores found in the HVF and SPF (but not the extracaldera GRF)

In addition to identifying the magmatic components involved in generating the SPF, the zircon and sanidine data provide constraints on the dynamics of the mixing event that formed the SPF magma. The fact that the SPF contains zircons characteristic of the main CPM reservoir (i.e., similar to HVF zircons) but lacks sanidines characteristic of the main CPM reservoir requires that either (1) the mixing component derived from the main CPM reservoir contained zircon but not sanidine or (2) all sanidines from the main reservoir component were completely resorbed during the mixing event. We favor the former scenario because sanidine crystallizes in nearly all Yellowstone rhyolites over a wide range of temperatures (e.g., ~750 to 900 °C for CPM rhyolites; Girard and Stix 2010; Vazquez et al. 2009; Watts et al. 2012) and therefore should be stable at any temperature in which zircon is stable (zircon saturation temperatures are typically <860 °C for CPM rhyolites; Watts et al. 2012). Thus, we consider it unlikely that all of the main CPM reservoir sanidines would completely dissolve without also dissolving the zircon from the main reservoir component. Instead, we suggest that the mixing component derived from the CPM reservoir was extracted as a zircon-bearing liquid from a crystal mush, while the sanidine remained behind in a locked crystal network (e.g., Claiborne et al. 2010a). Regardless of these considerations, the presence of SPF sanidine cores with Pb isotopic compositions between the HVF and SPF glasses suggests that these sanidine cores crystallized from a magma that was a mixture of main reservoir CPM magma and extracaldera magma, but with a larger proportion of the main reservoir component compared to the magma represented by the SPF glass (Figs. 13, 14). The systematic zoning from cores with low Ba, $^{208}Pb/^{206}Pb$, and $^{207}Pb/^{206}Pb$ (more similar to the HVF sanidine) to rims with higher Ba, $^{208}Pb/^{206}Pb$, and $^{207}Pb/^{206}Pb$ (similar to the SPF glass), combined with the fact that some SPF sanidines have multiple (up to four) zones of distinct composition with sharp contacts between each zone, suggests that compositional zoning in SPF sanidines records the composition of the SPF magma becoming progressively dominated by the extracaldera component through time (Figs. 13, 15). The similarity of the SPF glass to the GRF glass in trace-element composition and ε_{Hf} is consistent with the final mixture being dominated by the extracaldera component.

Although we cannot uniquely define how the mixing event that generated the SPF took place, we propose two scenarios that are consistent with the observations described above (Fig. 16). In one scenario the margin of the CPM reservoir and the adjacent extracaldera source rock are remelted by basaltic underplating and mixed prior to eruption, inheriting zircon from each source in the process (Fig. 16a). The idea of basalt being intimately involved in the generation of extracaldera rhyolites in consistent with the presence of mixed basalt–rhyolite complexes just north of the caldera margin, within ~15 km of the vent for the Gibbon River flow (e.g., Christiansen et al. 2007; Hildreth et al. 1991; Wooton 2010). In this scenario the lack of sanidines in the SPF that are characteristic of the main reservoir would be the result of dissolution of the main CPM reservoir sanidines. An alternative scenario is that the extracaldera magma was generated elsewhere (perhaps deeper in the system, e.g., Thomas and Watson 2012) and intersected the mushy margin of the CPM reservoir during ascent (Fig. 16b). As the silicic extracaldera magma flowed through the mushy CPM reservoir (e.g., Girard and Stix 2010), it mixed with the resident CPM magma and entrained zircons (but not sanidine) from the CPM reservoir. In either scenario, the mixed magma likely stalled temporarily before eruption, at least long enough for the major phases to crystallize (Fig. 16). As the mixing event(s) continued, more of the extracaldera component was added to the hybrid SPF magma until the SPF magma composition was dominated by the extracaldera (GRF-like) component. These mixing scenarios account for the zircon and sanidine populations present in the SPF, the zoning in Ba concentration and Pb isotopic composition observed in SPF sanidine, and the composition of the SPF glass relative to the CPM rhyolites.

The mixing between the main CPM reservoir and extracaldera rhyolites highlights the dynamic nature of magmatic interactions at the margin of the magma reservoir and represents a process by which compositionally diverse magmas can be produced that may be applicable to other silicic magma systems. Furthermore, these reservoir-margin mixing events may represent a process through which subtle chemical heterogeneities within the main reservoir are produced and "scatter" in the observed geochemical trends through time is generated (e.g., see scatter in trace element vs. eruption age plots in Vazquez et al. 2009 and Girard and Stix 2010). If mixing events like the one we propose here chemically modify local parts of the main reservoir, then different locations within the main reservoir may develop slight compositional differences depending on the local history of magma mixing, without altering the long-term thermochemical evolution of the system as a whole.

Origin and implications of high $^{176}Hf/^{177}Hf$ rhyolite at Yellowstone

In addition to constraining magma mixing associated with the formation of the SPF rhyolite, the zircon Hf isotopic data provide constraints on the sources of "main reservoir" rhyolitic magmas at Yellowstone. The HVF and SPF contain main reservoir-like zircons that are similar in

trace-element composition to zircons found in other main reservoir CPM rhyolites. Main reservoir-like zircons commonly have cores with high ε_{Hf} (−4 to 0) compared to the host CPM glass (−5.9 to −6.2 ε_{Hf}), but most rims have ε_{Hf} consistent with growth from the CPM reservoir. These data require that isotopically juvenile silicic magma(s) with Hf isotopic compositions (∼−4 to 0 ε_{Hf}) more primitive than the CPM glasses, older Yellowstone rhyolites, and the local crust is (or are) contributing liquid and zircon to the main CPM reservoir. In turn, these data (1) rule out the surrounding crust and all pre-CPM Yellowstone rhyolites—except potentially the Lava Creek Tuff ($\varepsilon_{Hf} = -1.1$; Nash et al. 2006)—as sources for the Hf isotopic heterogeneity observed in CPM zircons and (2) provide the first direct evidence of isotopically juvenile silicic magma (i.e., relative to erupted Yellowstone rhyolites and local crust) contributing mass to the post-caldera magmatic system at Yellowstone (Fig. 17). The observation of isotopically juvenile input into the system is consistent with suggestions by several researchers (e.g., Hildreth et al. 1991; Nash et al. 2006) that both isotopically evolved material (e.g., local crust) and isotopically juvenile material (i.e., akin to basalts) are required to explain the genesis of the CPM rhyolites, because the Nd isotopic compositions of the CPM rhyolites lie between that of the local crust and Yellowstone basalts (Fig. 17). If the isotopically juvenile silicic magma(s) that contributed the high ε_{Hf} zircons to the main CPM reservoir is (or are) the same component(s) responsible for driving the long-term evolution of the CPM reservoir to more juvenile Pb and Nd isotopic compositions (see Fig. 2), then all crustal sources and older Yellowstone rhyolites (including the Lava Creek Tuff) can be ruled out as the source for the juvenile silicic magmas because they do not have juvenile Pb and Nd isotopic compositions relative to the CPM glasses (Doe et al. 1982; Hildreth et al. 1991). Instead, the juvenile component in this scenario must be akin (at least partially) to Yellowstone basalts because they represent the only magmatic component at Yellowstone with the appropriate Pb and Nd isotopic composition to control the temporal trend in isotopic composition observed for the CPM rhyolites (Doe et al. 1982; Hildreth et al. 1991).

Two end-member models exist that offer an explanation of the source(s) being melted and/or fractionated to generate the high ε_{Hf} silicic magmas (and zircon). Hildreth et al. (1991) suggested that the source for Yellowstone rhyolites is a hybridized lower crust that consists of "mantle-derived components" with juvenile isotopic signatures (i.e., mantle-derived basalts, and fractionates or partial melts of mantle basalts) mixed with various "crustal components" (e.g., partial melts of basement rock and deep crustal granulites). In this model, partial melts of the hybridized lower crust, with radiogenic isotopic

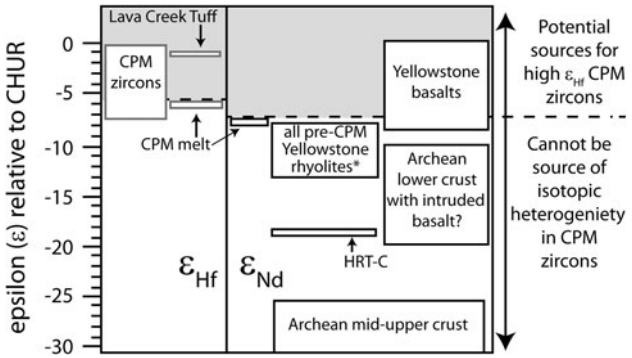

Fig. 17 Summary of Hf isotopic and Nd isotopic data for Yellowstone rhyolites, basalts, and local crust showing potential sources for the Hf isotopic heterogeneity observed in CPM zircons. The *x*-axis of the diagram is arbitrary. *Each box* shows the range of either Nd isotopic or Hf isotopic compositions for a given isotopic reservoir. *Gray boxes* located to the left of the vertical solid black line correspond to Hf isotopic compositions. *Black boxes* to the right of the *vertical solid black line* correspond to Nd isotopic compositions. The Nd and Hf isotopic compositions are reported in epsilon units calculated relative to CHUR at present (using $^{176}Hf/^{177}Hf_{CHUR(0)} = 0.282772$; $^{143}Nd/^{144}Nd_{CHUR(0)} = 0.512638$). * The field labeled "all pre-CPM Yellowstone rhyolites" includes the range of data for all main reservoir Yellowstone rhyolites (i.e., caldera-forming and intracaldera eruptions) erupted before the CPM rhyolites except for Huckleberry Ridge Tuff Member C (HRT-C), which shows evidence for large amounts of crustal assimilation and is plotted separately (see Hildreth et al. 1991). The gray field above the horizontal dashed line highlights the potential sources for the high ε_{Hf} CPM zircons. Note that the CPM zircons have a range of ε_{Hf} that extends to higher values than potential crustal sources and pre-CPM Yellowstone rhyolites (except the Lava Creek Tuff), indicating that these cannot be the sources for the isotopic heterogeneity observed in the CPM zircon. Only Yellowstone basalts and the Lava Creek Tuff have isotopic compositions similar to Yellowstone zircons. Where Hf isotopic data are not available, we consider Nd isotopic compositions as a rough proxy. Where both Hf and Nd isotopic data exist for Yellowstone samples, ε_{Hf} is typically 2–4 epsilon units higher than ε_{Nd} for a given eruptive unit (based on data from this study and Nash et al. 2006), and therefore, the general conclusions we make here are still valid when considering the expected differences between ε_{Hf} and ε_{Nd}. Note that the field highlighting the potential sources for the high ε_{Hf} CPM zircons has been corrected for the expected difference between ε_{Hf} and ε_{Nd} (based on data for the CPM glasses). Nd isotopic compositions of the crust (i.e., Archean mid-upper crust and Archean lower crust intruded with basalt) and the Hf isotopic composition of the Lava Creek Tuff are from Nash et al. (2006). Nd isotopic compositions of pre-CPM Yellowstone rhyolites (including HRT-C) are from Hildreth et al. (1991). Nd isotopic compositions of CPM rhyolites are from Vazquez et al. (2009). Nd isotopic compositions of the Yellowstone basalts are from Hildreth et al. (1991) and Bennett (2006)

compositions between that of Yellowstone basalts and the surrounding crust, ascend higher in the crust to accumulate and evolve further by crystallization and assimilation. In the context of this model, the main reservoir-like zircons with juvenile ε_{Hf} provide information about crystallization in juvenile melts derived from the hybridized lower crust. The zircons would then be carried along with the deeper,

juvenile rhyolites higher into the system where they experienced rim growth in a more contaminated level of the magmatic system that has experienced more assimilation of local crust and previously erupted intracaldera material (accounting for the less juvenile zircon rims).

The alternative model is one of shallow melting by basal heating from basaltic magmas. In this model the CPM rhyolites are the result of remelting buried intracaldera volcanic material and unerupted magmas from previous episodes of Yellowstone magmatism that are located within the dropped down intracaldera block (Bindeman et al. 2008; Watts et al. 2012). In the context of this model, the main reservoir-like zircons with juvenile ε_{Hf} would have crystallized from either (1) remelted high ε_{Hf} upper crustal material such as the Lava Creek Tuff ($\varepsilon_{Hf} = -1.1$; Nash et al. 2006) or (2) evolved silicic liquids derived from the underplated basalts, prior to being amalgamated into the main CPM reservoir. Other viable models for magma generation at Yellowstone exist that call upon different depths of rhyolite genesis and/or different proportions of "juvenile" versus "crustal" components (e.g., Leeman et al. 2008), but as the potential sources for the high ε_{Hf} silicic magmas remain the same, we do not discuss the other models in detail.

More generally, data from SPF, HVF, and GRF zircons demonstrate that zircons of similar age have a wide range of ε_{Hf} (Fig. 11). This suggests that the source region(s) in the crust that is generating and contributing rhyolitic magmas to the main CPM reservoir, whether located shallow or deep, is heterogeneous in $^{176}Hf/^{177}Hf$ at any given time. In turn, this implies that the relatively homogeneous liquid composition of erupted CPM rhyolites reflects homogenization of rhyolitic liquids within the magma reservoir instead of the homogeneous nature of the source rock or mush generating the rhyolites. Constraining whether isotopically juvenile rhyolite is continually added to the system will require additional work, including detailed U–Th–Hf analyses on zircons from other main reservoir CPM rhyolites erupted during different time periods.

Conclusions

1. Multiple crystal populations with distinct origins are observed within the coeval HVF and SPF based on: (a) subcrystal-scale age, trace-element, and Hf isotopic data from zircons hosted within the HVF, SPF, and GRF rhyolites and (b) major-element compositions, Ba concentrations, and Pb isotopic compositions of sanidines hosted within the HVF and SPF.
2. Comparing crystal populations between the SPF and HVF demonstrates that the HVF is derived from the main CPM reservoir while the SPF is a hybrid magma generated by mixing of a main CPM reservoir magma with extracaldera magma (similar to the GRF) at the margin of the CPM reservoir. This highlights the dynamic nature of magmatic interactions at the margin of the magma reservoir ca. 100 ka and represents a process by which compositional diversity in an eruptive suite can be produced that may be applicable to other silicic magma systems. This type of process may also contribute to the more subtle heterogeneities observed in the main reservoir.
3. More generally, the zircon data from the SPF and HVF provide the first direct evidence that juvenile (high ε_{Hf}) magma(s) is (or are) contributing zircon and liquid to the CPM reservoir. These data also demonstrate that the source regions in the crust that were generating and contributing rhyolitic magmas to the main CPM reservoir were heterogeneous in Hf isotopic composition ca. 100 ka, and therefore, the relatively homogeneous liquid composition of erupted CPM rhyolites reflects homogenization of rhyolitic liquids in the magma reservoir instead of the homogeneous nature of the source rock generating the rhyolites.

Acknowledgments We gratefully acknowledge support for this research through funding from National Science Foundation award EAR-1144945 to Kari Cooper and partial support from EAR-0738749 to Kari Cooper. We are also grateful for additional funding from National Science Foundation awards EAR-0538113 and EAR-0538309 to Mary Reid and Jorge Vazquez, Durrell research grants from UC Davis, and a GSA graduate student research grant to Mark Stelten. The ion microprobe facility at the University of California–Los Angeles is partly funded by a grant from the Instrumentation and Facilities Program, National Science Foundation. We would like to thank Nick Botto and Sarah Roeske for their help with electron microprobe analyses conducted at UC Davis, Michael Pantell and Allison Price for their help with laboratory work and sample preparation, Darren Tollstrup for his help with the zircon LA-MC-ICPMS analyses, Justin Glessner for his help with sanidine LA-MC-ICPMS analyses, and Axel Schmitt for his guidance during the zircon oxygen isotopic analyses at UCLA. We would also like to thank Kathryn Watts, two anonymous reviewers, and editor Jon Blundy for their constructive comments and suggestions that served to strengthen this manuscript.

References

Bachmann O, Miller CF, de Silva SL (2007) The volcanic–plutonic connection as a stage for understanding crustal magmatism. J Volcanol Geotherm Res 167(1–4):1–23

Bennett KM (2006) Petrogenesis of Pleistocene basalts in the Norris-Mammoth Corridor, Yellowstone National Park. MS thesis, University of Nevada, Las Vegas

Bindeman IN, Valley JW (2001) Low-delta O-18 rhyolites from Yellowstone: magmatic evolution based on analyses of zircons and individual phenocrysts. J Petrol 42(8):1491–1517

Bindeman IN, Fu B, Kita NT, Valley JW (2008) Origin and evolution of silicic magmatism at Yellowstone based on ion microprobe analysis of isotopically zoned zircons. J Petrol 49(1):163–193

Boroughs S, Wolff J, Bonnichsen B, Godchaux M, Larson P (2005) Large-volume, low-δ18O rhyolites of the central Snake River Plain, Idaho, USA. Geology 33(10):821–824

Burnham AD, Berry AJ (2012) An experimental study of trace element partitioning between zircon and melt as a function of oxygen fugacity. Geochim Cosmochim Acta 95:196–212

Carley T, Miller C, Wooden J, Bindeman I, Barth A (2011) Zircon from historic eruptions in Iceland: reconstructing storage and evolution of silicic magmas. Mineral Petrol 102(1):135–161

Cherniak DJ, Watson EB (2003) Diffusion in zircon. Rev Mineral Geochem 53(1):113–143

Christiansen RL (2001) The Quaternary and Pliocene Yellowstone Plateau volcanic field of Wyoming, Idaho, and Montana. US Geol Surv Prof Paper 729-G:145

Christiansen RL, Lowenstern JB, Smith RB, Heasler H, Morgan LA, Nathenson N, Mastin LG, Muffler LJP, Robinson JE (2007) Preliminary assessment of volcanic and hydrothermal hazards in Yellowstone National Park and vicinity. US Geol Surv Open File Rep 1071:1–98

Claiborne LL, Miller CF, Flanagan DM, Clynne MA, Wooden JL (2010a) Zircon reveals protracted magma storage and recycling beneath Mount St. Helens. Geology 38(11):1011–1014

Claiborne LL, Miller CF, Wooden JL (2010b) Trace element composition of igneous zircon: a thermal and compositional record of the accumulation and evolution of a large silicic batholith, Spirit Mountain, Nevada. Contrib Mineral Petrol 160(4):511–531

Crowley JL, Schoene B, Bowring SA (2007) U–Pb dating of zircon in the Bishop Tuff at the millennial scale. Geology 35(12): 1123–1126

Doe BR, Leeman WP, Christiansen RL, Hedge CE (1982) Lead and strontium isotopes and related trace-elements as genetic tracers in the Upper Cenozoic rhyolite-basalt association of the Yellowstone Plateau Volcanic Field. J Geophys Res 87(Nb6): 4785–4806

Gansecki CA, Mahood GA, McWilliams MO (1996) 40Ar39Ar geochronology of rhyolites erupted following collapse of the Yellowstone caldera, Yellowstone Plateau volcanic field: implications for crustal contamination. Earth Planet Sci Lett 142(1–2): 91–107

Girard G, Stix J (2009) Magma recharge and crystal mush rejuvenation associated with early post-collapse Upper Basin Member rhyolites, Yellowstone Caldera, Wyoming. J Petrol 50(11):2095–2125

Girard G, Stix J (2010) Rapid extraction of discrete magma batches from a large differentiating magma chamber: the Central Plateau Member rhyolites, Yellowstone Caldera, Wyoming. Contrib Mineral Petrol 160(3):441–465

Girard G, Stix J (2012) Future volcanism at Yellowstone caldera: insights from geochemistry of young volcanic units and monitoring of volcanic unrest. GSA Today 22(9):4–10

Hildreth W, Christiansen RL, Oneil JR (1984) Catastrophic isotopic modification of rhyolitic magma at times of caldera subsidence, Yellowstone Plateau Volcanic Field. J Geophys Res 89(Nb10): 8339–8369

Hildreth W, Halliday AN, Christiansen RL (1991) Isotopic and chemical evidence concerning the genesis and contamination of basaltic and rhyolitic magma beneath the Yellowstone Plateau Volcanic Field. J Petrol 32(1):63–138

Kemp AIS, Hawkesworth CJ, Foster GL, Paterson BA, Woodhead JD, Hergt JM, Gray CM, Whitehouse MJ (2007) Magmatic and crustal differentiation history of granitic rocks from Hf–O isotopes in zircon. Science 315(5814):980–983

Kent AJR (2008) In-situ analysis of Pb isotope ratios using laser ablation MC-ICP-MS: controls on precision and accuracy and comparison between Faraday cup and ion counting systems. J Anal At Spectrom 23(7):968–975

Klemetti EW, Deering CD, Cooper KM, Roeske SM (2011) Magmatic perturbations in the Okataina Volcanic Complex, New Zealand at thousand-year timescales recorded in single zircon crystals. Earth Planet Sci Lett 305(1–2):185–194

Lanphere MA, Champion DE, Christiansen RL, Izett GA, Obradovich JD (2002) Revised ages for tuffs of the Yellowstone Plateau volcanic field: assignment of the Huckleberry Ridge Tuff to a new geomagnetic polarity event. Geol Soc Am Bull 114(5): 559–568

Leeman WP, Annen C, Dufek J (2008) Snake River Plain—Yellowstone silicic volcanism: implications for magma genesis and magma fluxes. Geol Soc Lond Spec Publ 304(1):235–259

McCurry M, Rodgers DW (2009) Mass transfer along the Yellowstone hotspot track I: petrologic constraints on the volume of mantle-derived magma. J Volcanol Geotherm Res 188(1–3): 86–98

Miller JS, Wooden JL (2004) Residence, resorption and recycling of zircons in Devils Kitchen Rhyolite, Coso Volcanic Field, California. J Petrol 45(11):2155–2170

Nash BP, Perkins ME, Christensen JN, Lee DC, Halliday AN (2006) The Yellowstone hotspot in space and time: Nd and Hf isotopes in silicic magmas. Earth Planet Sci Lett 247(1–2):143–156

Pritchard C, Larson P (2012) Genesis of the post-caldera eastern Upper Basin Member rhyolites, Yellowstone, WY: from volcanic stratigraphy, geochemistry, and radiogenic isotope modeling. Contrib Mineral Petrol 164(2):205–228

Reid MR, Coath CD, Harrison TM, McKeegan KD (1997) Prolonged residence times for the youngest rhyolites associated with Long Valley Caldera: Th-230-U-238 ion microprobe dating of young zircons. Earth Planet Sci Lett 150(1–2):27–39

Reid MR, Vazquez JA, Schmitt AK (2011) Zircon-scale insights into the history of a Supervolcano, Bishop Tuff, Long Valley, California, with implications for the Ti-in-zircon geothermometer. Contrib Mineral Petrol 161(2):293–311

Schmitt AK (2006) Laacher See revisited: high-spatial-resolution zircon dating indicates rapid formation of a zoned magma chamber. Geology 34(7):597–600

Schmitt AK (2011) Uranium series accessory crystal dating of magmatic processes. Annu Rev Earth Planet Sci 39:321–349

Schmitt AK, Vazquez JA (2006) Alteration and remelting of nascent oceanic crust during continental rupture: evidence from zircon geochemistry of rhyolites and xenoliths from the Salton Trough, California. Earth Planet Sci Lett 252(3–4):260–274

Schoene B, Latkoczy C, Schaltegger U, Günther D (2010) A new method integrating high-precision U–Pb geochronology with zircon trace element analysis (U–Pb TIMS-TEA). Geochim Cosmochim Acta 74(24):7144–7159

Schoene B, Schaltegger U, Brack P, Latkoczy C, Stracke A, Günther D (2012) Rates of magma differentiation and emplacement in a ballooning pluton recorded by U–Pb TIMS-TEA, Adamello batholith, Italy. Earth Planet Sci Lett 355–356:162–173

Stelten ME, Cooper KM (2012) Constraints on the nature of the subvolcanic reservoir at South Sister volcano, Oregon from U-series dating combined with sub-crystal trace-element analysis of plagioclase and zircon. Earth Planet Sci Lett 313–314:1–11

Storm S, Shane P, Schmitt AK, Lindsay JM (2011) Contrasting punctuated zircon growth in two syn-erupted rhyolite magmas from Tarawera volcano: insights to crystal diversity in magmatic systems. Earth Planet Sci Lett 301(3–4):511–520

Storm S, Shane P, Schmitt A, Lindsay J (2012) Decoupled crystallization and eruption histories of the rhyolite magmatic system at Tarawera volcano revealed by zircon ages and growth rates. Contrib Mineral Petrol 163(3):505–519

Tappa MJ, Coleman DS, Mills RD, Samperton KM (2011) The plutonic record of a silicic ignimbrite from the Latir volcanic field, New Mexico. Geochem Geophys Geosyst 12(10):Q10011

Thomas J, Watson EB (2012) Application of the Ti-in-quartz thermobarometer to rutile-free systems. Reply to: a comment on: 'TitaniQ under pressure: the effect of pressure and temperature on the solubility of Ti in quartz' by Thomas et al. Contrib Mineral Petrol 164(2):369–374

Tollstrup DL, Xie LW, Wimpenny JB, Chin E, Lee CT, Yin QZ (2012) A trio of laser ablation in concert with two ICP-MSs: simultaneous, pulse-by-pulse determination of U–Pb discordant ages and a single spot Hf isotope ratio analysis in complex zircons from petrographic thin sections. Geochem Geophy Geosy 13:1–14

Trail D, Mojzsis SJ, Harrison TM, Schmitt AK, Watson EB, Young ED (2007) Constraints on Hadean zircon protoliths from oxygen isotopes, Ti-thermometry, and rare earth elements. Geochem Geophys Geosyst 8(6):Q06014

Trail D, Bruce Watson E, Tailby ND (2012) Ce and Eu anomalies in zircon as proxies for the oxidation state of magmas. Geochim Cosmochim Acta 97:70–87

Valley JW (2003) Oxygen isotopes in zircon. Rev Mineral Geochem 53:343–385

Vazquez JA, Reid MR (2002) Time scales of magma storage and differentiation of voluminous high-silica rhyolites at Yellowstone caldera, Wyoming. Contrib Mineral Petrol 144(3):274–285

Vazquez JA, Kyriazis SF, Reid MR, Sehler RC, Ramos FC (2009) Thermochemical evolution of young rhyolites at Yellowstone: evidence for a cooling but periodically replenished postcaldera magma reservoir. J Volcanol Geotherm Res 188(1–3):186–196

Vervoort JD, Blichert-Toft J (1999) Evolution of the depleted mantle: Hf isotope evidence from juvenile rocks through time. Geochim Cosmochim Acta 63(3–4):533–556

Watts KE, Leeman WP, Bindeman IN, Larson PB (2010) Supereruptions of the Snake River Plain: two-stage derivation of low-δ18O rhyolites from normal-δ18O crust as constrained by Archean xenoliths. Geology 38(6):503–506

Watts K, Bindeman I, Schmitt A (2012) Crystal scale anatomy of a dying supervolcano: an isotope and geochronology study of individual phenocrysts from voluminous rhyolites of the Yellowstone caldera. Contrib Mineral Petrol 164(1):45–67

White SM, Crisp JA, Spera FJ (2006) Long-term volumetric eruption rates and magma budgets. Geochem Geophys Geosyst 7(3): Q03010

Wiedenbeck M, Hanchar JM, Peck WH, Sylvester P, Valley J, Whitehouse M, Kronz A, Morishita Y, Nasdala L, Fiebig J, Franchi I, Girard JP, Greenwood RC, Hinton R, Kita N, Mason PRD, Norman M, Ogasawara M, Piccoli PM, Rhede D, Satoh H, Schulz-Dobrick B, Skår O, Spicuzza MJ, Terada K, Tindle A, Togashi S, Vennemann T, Xie Q, Zheng YF (2004) Further characterisation of the 91500 zircon crystal. Geostand Geoanal Res 28(1):9–39

Wolff JA, Ramos FC (2003) Pb isotope variations among Bandelier Tuff feldspars: no evidence for a long-lived silicic magma chamber. Geology 31(6):533–536

Wooton KM (2010) Age and petrogenesis of the Roaring Mountain rhyolites, Yellowstone Volcanic Field, Wyoming. MS thesis, University of Nevada, Las Vegas